

Frontiers of Information Technology & Electronic Engineering  
 www.jzus.zju.edu.cn; engineering.cae.cn; www.springerlink.com  
 ISSN 2095-9184 (print); ISSN 2095-9230 (online)  
 E-mail: jzus@zju.edu.cn



## Review:

# Displacement measuring grating interferometer: a review<sup>\*</sup>

Peng-cheng HU<sup>1,2</sup>, Di CHANG<sup>1,2</sup>, Jiu-bin TAN<sup>†‡1,2</sup>, Rui-tao YANG<sup>1,2</sup>, Hong-xing YANG<sup>1,2</sup>, Hai-jin FU<sup>1,2</sup>

<sup>1</sup>Center of Ultra-precision Optoelectronic Instrument Engineering, Harbin Institute of Technology, Harbin 150080, China

<sup>2</sup>Key Lab of Ultra-precision Intelligent Instrumentation, Ministry of Industry and Information Technology, Harbin 150080, China

<sup>†</sup>E-mail: jbtan@hit.edu.cn

Received Nov. 7, 2018; Revision accepted Feb. 23, 2019; Crosschecked May 8, 2019

**Abstract:** A grating interferometer, called the “optical encoder,” is a commonly used tool for precise displacement measurements. In contrast to a laser interferometer, a grating interferometer is insensitive to the air refractive index and can be easily applied to multi-degree-of-freedom measurements, which has made it an extensively researched and widely used device. Classified based on the measuring principle and optical configuration, a grating interferometer experiences three distinct stages of development: homodyne, heterodyne, and spatially separated heterodyne. Compared with the former two, the spatially separated heterodyne grating interferometer could achieve a better resolution with a feature of eliminating periodic nonlinear errors. Meanwhile, numerous structures of grating interferometers with a high optical fold factor, a large measurement range, good usability, and multi-degree-of-freedom measurements have been investigated. The development of incremental displacement measuring grating interferometers achieved in recent years is summarized in detail, and studies on error analysis of a grating interferometer are briefly introduced.

**Key words:** Grating interferometer; Optical encoder; Displacement measurement; Precision measurement

<https://doi.org/10.1631/FITEE.1800708>

**CLC number:** TH744.3; TH822

## 1 Introduction

During the past century, science and technology have significantly advanced, reaching an unprecedented level, and will progress further. As an example, the length of the scale of precision machining and measurement devices has been driven by an increasing trend toward precision, breaking through the nanometer, sub-nanometer, and even picometer scales from the scale of several microns achieved in 1900 (Riemer, 2011; Yuan et al., 2017). The improvement in scale has led to many sophisticated products, such as high performing mechanical components and high

density integrated circuits (ICs), which are cornerstones of today’s nano-era and information age.

Semiconductor technology might be the most advanced technology that best reflects the level of precision. At present, there are billions of electronic devices in the world that together make up the Internet of Things (IoT), and countless semiconductor chips are constantly working with high reliability and accurately performing simple or complex functions. Since the birth of the first IC in 1958, ICs have been miniaturized, complicated, and commercialized (Kilby, 2000; Lee, 2007). Beginning at 764  $\mu\text{m}$ , which was the size of the first commercial planar transistor in the early 1960s, the critical dimensions (CDs) of ICs reached the submicron scale by the turn of the century. Because CDs have been reduced under 10 nm throughout the years, a new prediction called “more than Moore” has been recently proposed, and the microstructure of ICs has gradually turned from planar designs to denser three-dimensional (3D) designs (Ramm et al., 2010; Badaroglu et al., 2014;

<sup>‡</sup> Corresponding author

<sup>\*</sup> Project supported by the National Natural Science Foundation of China (Nos. 51605120, 51675138, and 61675058) and the National Science and Technology Major Project, China (No. 2017ZX02101006-005)

ORCID: Peng-cheng HU, <http://orcid.org/0000-0002-2471-7036>  
 © Zhejiang University and Springer-Verlag GmbH Germany, part of Springer Nature 2019

Richardson et al., 2017). All of these technological innovations have allowed today's portable smart electronic devices to be developed; however, at the same time, they have placed extremely demanding requirements on the lithography. A wafer stage, a key component in the lithography machine, is used to carry and move the wafer or to keep it at a predetermined position for exposure. In general, a wafer stage will have 3–6 degrees of freedom (DOF) of motion. The accuracy requirements of translational motions will increase as the CD decreases (Damm et al., 2001; Lan et al., 2007). For instance, currently used double-exposure techniques now permit a CD overlay error of no more than 15% with approximately 20% allocated for the stage metrology (Schmidt, 2012). Meanwhile, the moving speed of the wafer stage is at a level of several meters per second. Achieving high-precision sub-nanometer displacement measurements of multi-DOF motions at such a high speed is a significant challenge for metrology. It is important that the multi-DOF measurement results of the wafer stage be used as the inputs of the control system, closely relating to its motion control accuracy and even exposure quality. Therefore, the multi-DOF high-precision nano-positioning and measurement system of the high-speed wafer stage is an indispensable part of a lithography machine.

In general, to achieve such a high-precision nano-scale relative displacement measurement, common solutions, including the use of a laser interferometer, a grating interferometer (GI, also called an “optical encoder”), a capacitive sensor, or a linear variable differential transformer (LVDT), can be divided into two categories: optical and electrical methods. As shown in Table 1, among the solutions mentioned above, electrical methods are used for mainly short-range measurements within several millimeters because of the principle limitation. However, optical methods are advantageous in measuring the accuracy, resolution, and range, and

have become the preferred methods for high-precision displacement measurements.

A comparison of the two classical optical techniques for precise displacement measurements, namely, the use of a laser interferometer or a GI, has continued to be made (Teimel, 1991; Kunzmann et al., 1993; Badami and de Groot, 2013). At present, the displacement measurement accuracy of both methods can reach the sub-nanometer or picometer scales (Bai et al., 2017; Deng et al., 2018; Hori et al., 2018). Both methods are categorized as optical interference methods, and have many similarities in principle and structure. The main difference of them lies in the measuring benchmarks.

Table 2 shows that the measurements using a laser interferometer are based on the wavelength, which is traceable but sensitive to the air refractive index. Thus, high-precision air refractive index compensation is required (Jang and Kim, 2017). In contrast, the pitch of the grating is insensitive to barometric pressure and humidity. In addition, the application of materials with low thermal expansion coefficients, such as invar and glass ceramics, can greatly decrease the thermal expansion caused by temperature fluctuations (Hsu et al., 2013; Hossein et al., 2016). Therefore, a GI maybe suitable for industrial measurements owing to its insensitivity to environmental disturbances. In a lithography machine with a decline of the CD, the correlation analysis shows that over 80% of the total errors are related to the influence of the air fluctuations on a laser interferometer (de Groot et al., 2016). A GI, as a substitute for a laser interferometer, has already been used in photolithography to monitor the critical platform motion during the wafer exposure step (Shibazaki et al., 2009).

With regard to the measurement range, a laser interferometer is absolutely superior. Arms used in a laser interferometer for a gravitational-wave measurement can reach tens of meters or even several

**Table 1 Solutions for high-precision relative displacement measurements**

Category	Method	Feature
Optical	Laser interferometer	Extremely high range; traceability; sensibility to air refraction index
	Grating interferometer	Ranging from several millimeters to meters; resistance to ambient turbulence; influence of ruling errors
Electrical	Capacitive sensor	Insensibility to air refraction index; short range in millimeters; influenced by side effects
	LVDT	Insensibility to temperature; lower resolution than other comparable methods; restriction from large sized cores and armature

**Table 2 A comparison between grating interferometers and laser interferometers**

	Grating interferometer	Laser interferometer
Measuring benchmark	The benchmark is at a scale of several hundred nanometers to micrometers; not affected by air refractive index; the use of zero thermal expansion materials can resist temperature changes. Affected by the ruling error and needs to be calibrated.	The benchmark is the wavelength of the laser, which can be used as a length reference in a vacuum environment. Harsh environmental requirements; the effects of air refractive index (temperature, humidity, and pressure) need to be compensated for.
Length and dimension	The length ranges from tens of millimeters to tens of meters (Dr. Johannes Heidenhain GmbH, 2018); the two-DOF synchronous measurement can be realized through planar grating. The size of the planar grating is within 100–200 m.	It is easy to measure the displacement at the meter scale; the length of the arms can reach up to the kilometer scale. The structure of a multi-DOF measurement is complex.
Measurement accuracy	Measurement accuracy of the sub-nanometer level can be achieved through phase subdivision and calibration.	In addition to a phase subdivision, the measurement accuracy of the sub-nanometer or even picometer scales can be achieved through an air refractive index compensation and the creation of a vacuum environment.

kilometers in length, such as the most famous LIGO (Goßler et al., 2010; Cho, 2016). However, an enhancement of the optical configuration for multi-DOF measurements of a laser interferometer is not as convenient as a GI. The difference here can be attributed to the orientations of the benchmarks and the laser beams. Clearly, as the benchmark of a laser interferometer, the wavelength is parallel with the laser beam, which means that a laser interferometer must have several sub-systems placed around the measured stage for measuring the motions in different directions (Gao, 2010; Lazar et al., 2010; Gao et al., 2013). However, the grating pitch is always located vertically or at a certain angle to the incident lasers. Therefore, with a single grating, GIs can achieve up to six-DOF measurement in a compact area (Schwenke et al., 2002; Cosijns and Jansen, 2014).

These advantages of a GI mentioned above have resulted in increasing attention from researchers, manufacturers, and users. As Figs. 1 and 2 show, relevant investigations provide a confirmation that in both North America and Japan the proportion of grating encoders has shown a continuous and significant upward trend since 1994 (Lee and Lee, 2013; Gao et al., 2015).

At the same time, researchers are deeply exploring and improving the use of GIs in several aspects. We summarize the use of GIs in recent years in terms of the principal optical structure for a good performance and multi-DOF measurements, and an error analysis, while particularly focusing on the incremental GIs at nanometer and sub-nanometer resolutions.

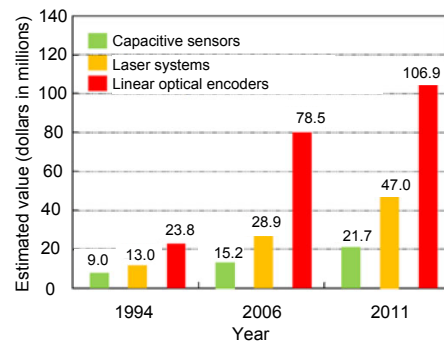


**Fig. 1 Market share of linear displacement measuring sensor in the VDC company in North America (reprinted from Lee and Lee (2013), Copyright 2013, with permission from Springer Nature)**

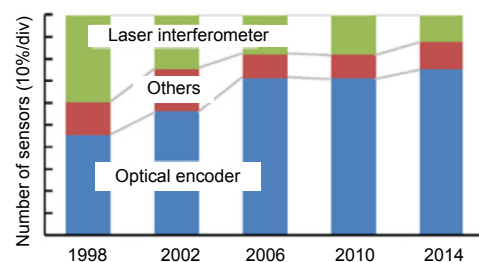


**Fig. 2 Japan society of professional engineers: changes in the proportion of precision positioning sensors (reprinted from Gao et al. (2015), Copyright 2015, with permission from Elsevier)**

## 2 Principle and optical structure

The term grating interferometer was not new when the laser was invented (Ronchi, 1964). However,

a laser and its good coherence have achieved a good performance combined with a GI. Similar to laser interferometers, the development of GI has experienced an exploration from homodyne and heterodyne interferometry to spatially separated heterodyne interferometry.

## 2.1 Homodyne grating interferometer

As the earliest and the most widely used interferometry, homodyne interferometry uses a single-frequency laser source. A Michelson-type homodyne GI is shown in Fig. 3a. The single-frequency laser beam with a frequency of  $f$  is divided into two parts by a non-polarized beam splitter (NPBS), which enters the measuring and reference arms and becomes the measuring and reference beams, respectively. The measuring beam is diffracted by the measuring grating, and the reference beam is diffracted by the reference grating. These two diffracted beams are deflected by the refractive components and transmitted to a photodetector module after converging in the NPBS. The single photodetector shown in Fig. 3b can realize only homodyne interference displacement measurements without distinguishing the direction of motion (Ellis, 2014). To achieve direction sensitivity, a quadratic phase detector module and a quadrature phase detector module, as shown in Figs. 3c and 3d, respectively, are required.

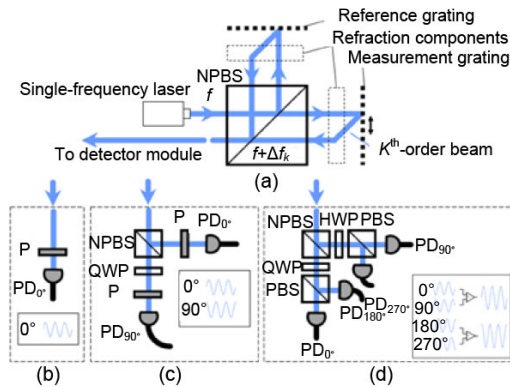


**Fig. 3** A homodyne grating interferometer in a Michelson-type structure: (a) an optical structure of reading head; (b) a single photodetector; (c) a quadratic phase detector module; (d) a quadrature phase detector module. NPBS: non-polarized beam splitter; P: polaroid; PD: photodetector; QWP: quarter wave-plate; HWP: half wave-plate

Similar to the reference and measurement mirrors in a Michelson-type laser interferometer, a

Michelson-type GI contains a fixed reference grating and a moving measuring grating. In general, owing to the outward divergence of the diffracted beams, an additional pair of refractive components is usually placed to turn the divergent beams into parallel beams, reducing the spatial volume of the optical configuration. Common refractive devices include a convex lens (Gao and Kimura, 2007), mirrors (Wang et al., 2014), a transmission grating that has the same period as a measuring grating (Kimura et al., 2012; Ito et al., 2014; Shimizu et al., 2014; Lin et al., 2017; Zherdev et al., 2017), and prisms (Kimura et al., 2010a, 2010b; Li et al., 2013). Strictly speaking, the function of the reference grating is to simply generate the reference beams in specific spatial locations corresponding to the measuring beams. Therefore, it is possible to replace the reference grating and refractive devices using a group of optical components, such as prisms or corner-cube retro-reflectors (Zhu et al., 2014, 2018).

When the measuring grating moves, the diffraction beams generated on its surface will incur frequency shifts because of the optical Doppler effect, resulting in a phase difference between the reference beam (reference signal) and the measuring beam (measurement signal) (Cloud, 2005; Wise et al., 2005).

As shown in Fig. 3a, the wave equation of the beam emitted by the laser is expressed as

$$E_0 = A_0 \cos(2\pi ft + \varphi_0), \quad (1)$$

where  $A_0$  is the amplitude and  $\varphi_0$  is the initial phase. When the beam passes through a fixed reference grating, the frequency characteristic does not change, and the wave equation of the reference beam is expressed as

$$E_r = A_r \cos(2\pi ft + \varphi_r), \quad (2)$$

where  $A_r$  and  $\varphi_r$  are the amplitude and phase, respectively. Through the modulation of a moving measuring grating, we can obtain the wave equation of the measuring beam as

$$\begin{aligned} E_m &= A_m \cos[2\pi(f + \Delta f_k)t + \varphi_m] \\ &= A_m \cos(2\pi ft + 2\pi Ks/g + \varphi_m), \end{aligned} \quad (3)$$

where  $s$  is the measured displacement,  $g$  the grating constant, and  $\varphi_m$  the additional phase caused by the optical path of the measurement arm. The optical fold factor  $K$  will be discussed in Section 3.1.

When two beams synthesize the interference beam, the wave equation is  $E_r + E_m$ , and the electrical signal collected by the photoelectric detector is theoretically proportional to the interference intensity  $(E_r + E_m)^2$ . Owing to the limitation of the device response band, the photoelectric detector actually obtains information with a lower frequency, expressed as

$$I \propto A_r^2 + A_m^2 + 2A_r A_m \cos(2\pi ks/g). \quad (4)$$

Therefore, the actual motion phase can be extracted by orthogonal phase signals, and the length and direction of the grating displacement can be calculated. Although the quadrature phase detector module in Fig. 3d is complex and bulky in its structure, it can eliminate DC bias by providing differential signals and has become a common detector form of a homodyne GI (Fan et al., 2006; Kimura et al., 2012; Lin et al., 2015; Li et al., 2017).

A homodyne GI has been widely used because of its simple structure and the few laser sources required. However, it is sensitive to stray light, and the phase-sensitive detector requires a complex optical structure containing multiple PDs (Ellis, 2014).

### 2.2 Heterodyne grating interferometer

To solve the problem of homodyne GI, heterodyne technology is applied to grating interferometry, resulting in a heterodyne GI. In contrast to the only frequency used in the homodyne interferometry, the term “heterodyne” signifies a dual-frequency laser source.

As shown in Fig. 4, a heterodyne GI can form a Michelson-type structure. The dual-frequency laser orthogonally emits a polarized laser with frequencies of  $f_1$  and  $f_2$  (assuming  $f_1 > f_2$ ). First, the beam is divided into two parts in the NPBS, where the reflected beam is interfered by the detector and a reference signal is formed after being measured by PD<sub>r</sub>. Then the transmission beam is divided into two parts based on the polarization at the interface of a polarized beam splitter (PBS), which respectively enter the reference and measuring gratings. Similar to the diffraction

discussed in Section 2.1, the measuring beam’s  $k^{\text{th}}$ -order diffraction beam with a Doppler frequency shift returns to the PBS through the refractive component and converges with the corresponding reference beam. Finally, the measuring beam obtained through the interferometer is collected by PD<sub>m</sub>. For a heterodyne GI, the frequency difference of  $f_1 - f_2$  can be regarded as the carrier of displacement information, which makes it possible to discern the direction using a single PD (Ellis, 2014). However, it should be made clear that the value of the carrier frequency determines the theoretically measurable range of Doppler frequency shifts, or in other words, the range of the moving velocity.

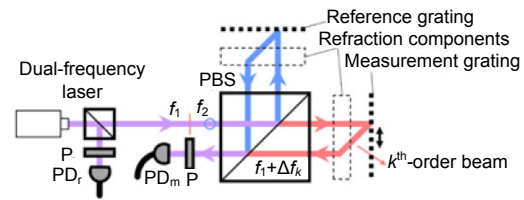


**Fig. 4** A heterodyne grating interferometer in a Michelson-type structure

Wave equations corresponding to the two frequency components of an orthogonal dual-frequency polarized laser can be expressed as

$$E_1 = A_1 \cos(2\pi f_1 t + \varphi_1), \quad (5)$$

$$E_2 = A_2 \cos(2\pi f_2 t + \varphi_2), \quad (6)$$

where  $A_1$  and  $A_2$  are the amplitude coefficients, and  $\varphi_1$  and  $\varphi_2$  are the initial phases. Passing through a reference prism, wave equations of the two components in the reference arm are expressed as

$$E_{1r} = A_{1r} \cos(2\pi f_1 t + \varphi_{1r}), \quad (7)$$

$$E_{2r} = A_{2r} \cos(2\pi f_2 t + \varphi_{2r}). \quad (8)$$

Thus, the intensity of the reference beam detected by PD<sub>r</sub> is  $E_{1r} + E_{2r}$ , expressed as

$$I_r \propto A_{1r}^2 + A_{2r}^2 + 2A_{1r} A_{2r} \cos[2\pi(f_1 - f_2)t]. \quad (9)$$

Wave equations of the two components in the measuring arm are respectively expressed as

$$E_{1m} = A_{1m} \cos[2\pi(f_1 + \Delta f_k)t + \varphi_{1m}], \quad (10)$$

$$E_{2m} = A_{2m} \cos(2\pi f_2 t + \varphi_{2m}). \quad (11)$$

Similarly, intensity acquired by PD<sub>m</sub> can be expressed as

$$I_m \propto A_{1m}^2 + A_{2m}^2 + 2A_{1m}A_{2m} \cos[2\pi(f_1 - f_2)t + 2\pi Ks/g]. \quad (12)$$

The function of the signal processing module is to demodulate the corresponding displacement information from the measuring signal  $I_m$  (Eq. (12)), using the carrier information  $I_r$  in Eq. (9) as a reference.

Compared with a Michelson-type structure (Wang et al., 2014; Zhu et al., 2014, 2018), another structure with a single grating is more commonly used (Lee et al., 2007; Lin et al., 2015b; Yan et al., 2015). Because the grating diffraction produces multiple orders of diffracted beams with different Doppler frequency shifts, the measuring signal can be obtained through the interference between diffracted beams in different orders of a single grating. As Fig. 5a shows, the  $\pm$ first-order diffraction beams of a normally incident beam converge and generate an interference beam. In Fig. 5b, the beam emitted by the laser source is divided into two parts, and then the diffraction beams of these two beams interfere with each other. These two methods with a single-grating structure can form differential signals to improve the resolution. Details will be described in Section 3.1.

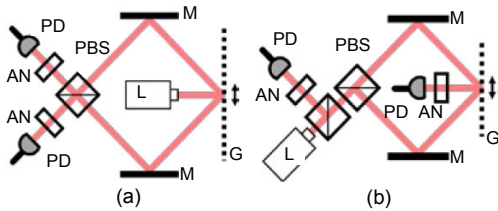


**Fig. 5 A heterodyne grating interferometer in single-grating structures with a vertical incident beam (a) and with symmetrical oblique incident beams (b)**

L: dual-frequency laser; G: grating; M: mirror; PBS: polarized beam splitter; AN: analyzer; PD: photodetector

As mentioned above, one of the advantages of a heterodyne GI is that it can distinguish direction using a single PD. In addition, the high signal-to-noise ratio (SNR) brought by the carrier signal greatly improves

the measurement accuracy. However, compared with a homodyne GI, a heterodyne GI is more demanding in terms of the dual-frequency laser source and the demodulated part of signal processing. More complicated than a single-frequency laser, a heterodyne GI usually requires an internal modulation laser, such as a dual-frequency Zeeman laser (Asano et al., 2001; Wang et al., 2014; Lin et al., 2015b) or a semiconductor laser with a modulated voltage (Hsieh et al., 2014). Substitutions include an external modulation laser equipped with an electro-optical modulator (EOM) (Lee et al., 2007), an acousto-optical modulator (AOM) (Heilmann et al., 2004; Guan et al., 2017; Xing et al., 2017), and other devices. In addition, demodulation of the signals needs to be programmed in the signal processing module.

In addition to these devices and algorithm requirements, the combination of a heterodyne interferometry and a GI brings about a large problem called a “periodic nonlinear error.” Because of the optical mixing phenomenon caused by the imperfect splitting performance of the PBS, a periodic nonlinear error of several to tens of nanometers is found in a heterodyne grating interferometer (Lin et al., 2000; Hsieh et al., 2010; Fu et al., 2018b).

For instance, when the leakage of an actual PBS, shown in Fig. 4, is taken into account, the resulting wave equations of the transmitted and reflected beams can be expressed as

$$E_t = A_t \cos(2\pi f_1 t + \varphi_{1t}) + a_t \cos(2\pi f_2 t + \varphi_{2t}), \quad (13)$$

$$E_r = a_r \cos(2\pi f_1 t + \varphi_{1r}) + A_r \cos(2\pi f_2 t + \varphi_{2r}). \quad (14)$$

where  $A_t$ ,  $A_r$ ,  $a_t$ , and  $a_r$  reveal the extents of a polarization leakage.

Therefore, after a Doppler frequency shift, the interference of two beams with optical mixing will generate a measurement signal with periodic nonlinear errors, expressed as

$$I_m \propto I_{DC} + A_t A_r \cos[2\pi(f_1 - f_2 + \Delta f_k)t] + (A_t a_r + A_r a_t) \cdot \cos[2\pi(f_1 - f_2)t] + a_t a_r \cos[2\pi(f_1 - f_2 - \Delta f_k)t]. \quad (15)$$

The existence of the periodic nonlinear errors is a barrier, preventing the resolution of a GI from further developing to the sub-nanometer level.

### 2.3 Spatially separated heterodyne grating interferometer

Common approaches used to break through the limitation of periodic nonlinear errors include passive compensation and active elimination. Because of the similarity in principle, the periodic nonlinear error compensation method used for heterodyne laser interferometers is suitable for heterodyne GIs (Hou et al., 2009; Kim et al., 2012; Xie et al., 2017). As a theoretical elimination of the periodic nonlinear errors, a spatially separated heterodyne GI was first proposed by Hu et al. (2014) and Tan et al. (2014). Configurations of spatially separated heterodyne GIs are shown in Fig. 6. In addition to the Michelson-type and normally incident single-grating structures, Zhang et al. (2017) designed a Littrow configuration of a spatially separated heterodyne GI, and Guan et al. (2017) proposed a single-grating structure with a pair of symmetrical oblique beams. Because the two beams are split at different locations, optical mixing caused by the imperfect performance of the PBS can be avoided. Optical configuration of the spatial separation is a key to eliminating periodic nonlinear errors, and its effect was practically tested.

As shown in Fig. 7a, a comparative experiment using frequency spectrum analysis verified that the measuring signal of a spatially separated heterodyne GI is close to the ideal PBS in Eq. (12), avoiding the optical mixing in heterodyne common-optical-path structures in Eq. (15) (Xing et al., 2017). When the grating is at rest, the frequency difference is equal to 5 MHz. The spectral peak corresponding to the

nonlinear error of the common-optical-path structure as the grating moves can be clearly seen in the left curve of Fig. 7b. The elimination of nonlinear errors in the spatially separated structure is shown in the right curve of Fig. 7b.

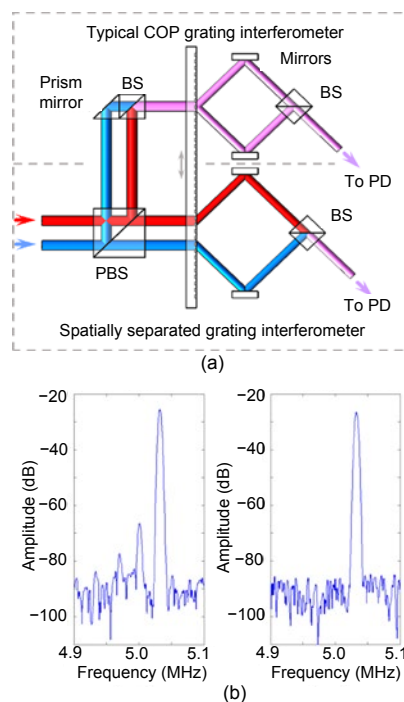


**Fig. 7 A comparison of nonlinear errors between spatially separated structures and common-optical path structures using frequency spectrum analysis: (a) experimental setup; (b) spectrum curves acquired using a signal analyzer: common-optical path structure (left) and spatially separated structure (right) (reprinted from Xing et al. (2017), Copyright 2017, with permission from the Optical Society)**

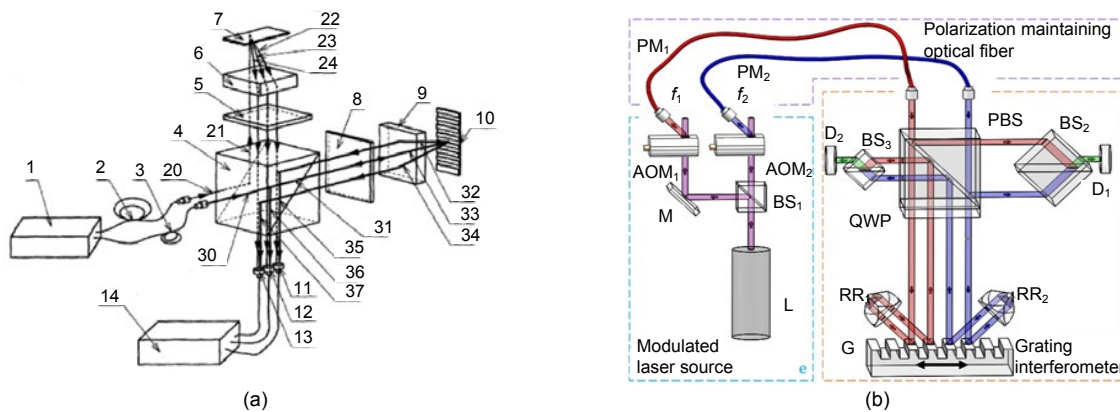


**Fig. 6 Spatially separated heterodyne grating interferometer structures: (a) a Michelson-type structure; (b) a single-grating structure with a pair of vertical incident beams (reprinted from Xing et al. (2017), Copyright 2017, with permission from the Optical Society)**

As a recently proposed concept, the spatially separated heterodyne grating interferometer still requires further investigation and application. For instance, because the separation of beams complicates the optical configuration, a delicate and stable optical design is important for wide application. Power loss caused by AOM and fiber needs further consideration for an optimum.

### 3 Structures for good performance

Basic principles and structures of three types of GIs have been introduced above; however, it is insufficient to realize precise displacement measurements using these basic optical configurations. In recent years, researchers have delivered a variety of studies on advanced optical structures of GIs to obtain a good performance. The major performance improvements include a high resolution, a large range, and good usability.

#### 3.1 Optical structures for high resolution

According to the equations given in Section 2, the relationship between grating displacement and phase change in an interference signal can be expressed as follows:

$$\Delta\varphi = 2\pi Ks/g. \quad (16)$$

A main way to improve the resolution is to increase the phase change caused by the same displacement, specifically, to decrease the grating constant  $g$  or to increase the optical fold factor  $K$  (the electrical interpolation factor in the signal processing module will be discussed in Section 5.3). With an improvement in fabrication, the grating enters a generation of holographic grating from ruling grating, and the grating pitch and ruling error are further decreased. Grating used in the early interferometer was typically tens of microns. However, in recent years, the constant of high-density gratings has reached a micron scale, which can easily achieve 1000 lines/mm or higher (Schwenke et al., 2002; Deng et al., 2018). Decreasing the grating pitch is the simplest way to improve the resolution of a GI (Jiang et al., 2013), but it is limited by the grating equation. For the same beam source, the reduction of grating constant

will result in an increase in the diffraction angle, and is eventually constrained by the right angle limitation. Thus, the main approach to improve the optical resolution focuses on increasing the optical fold factor.

In general, grating diffraction will produce diffracted beams in positive and negative orders with opposite Doppler frequency shifts and a zeroth-order diffracted beam without a Doppler frequency shift. Therefore, interference by diffracted beams of different orders can form a single structure (e.g., interference by the zeroth- and first-order beams) or a differential structure (e.g., interference by  $\pm$ first-order beams) (Hsieh et al., 2011). A differential structure is the most commonly used method to improve the resolution, because it can improve the optical fold factor without increasing the optical components. For instance, compared with the single structure in Fig. 4, optical fold factors are doubled in differential structures (Fig. 5).

In the case of a multi-order diffracted beam, the interference of a high-order diffracted beam can be used to increase the optical fold factor. For example, the optical resolution can be raised to  $2 \times m$  with the interference by a pair of  $\pm m^{\text{th}}$ -order diffracted beams. Specifically, as shown in Fig. 8, in a triple grating combined with an interferometer, the optical fold factor is four when it is interfered with  $\pm$ second-order diffracted beams (Hsu et al., 2017, 2018). In addition, Chu et al. (2008) achieved an optical fold factor of 10 by  $\pm$ fifth-order diffracted beams. However, the

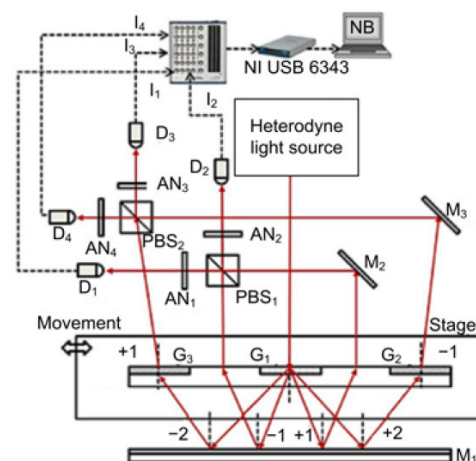


Fig. 8 Differential structure with  $\pm$ second-order diffracted beams in a triple grating combination interferometer (reprinted from Hsu et al. (2017), Copyright 2017, with permission from the Optical Society)

greatest deficiency of this approach lies in the low efficiency of a high-order diffracted beam, generating interference signals with an unwarranted low SNR. As an available compensative approach, the diffraction efficiency of certain diffraction orders could be strengthened by a blazed or special designed grating (Post, 1971; Williams et al., 2017).

Based on a differential optical structure, an enhancement of the optical resolution through a multi-fold increase in diffraction of  $\pm$ first-order diffracted beams is another commonly used approach. Multi-fold diffraction means that the diffracted beams are reflected to the grating and diffract each time. Theoretically, the more diffractions the beams experience, the larger the optical fold factor is. In general, because of a limitation of the grating diffraction efficiency, the diffraction order is typically set to two. As shown in Fig. 9, there are several methods used to realize double-diffractions, including mirrors (Lee and Jiang, 2013; Zhao et al., 2015), convergent lens and mirrors (Lee et al., 2004; Kao et al., 2005a; Hsu et al., 2009), reflection prisms (Wang et al., 2004; Jiang et al., 2011, 2012), and retroreflectors (Kao et al., 2005b; Fan et al., 2006; de Groot and Schroeder, 2012; Feng et al., 2013; Deck et al., 2015). In addition, specially designed optical components have been proposed for large fold factors. For example, Deng et al. (2018) designed a special prism, called a “high optical subdivision module” (HOSM), implemented in an eight-fold optical configuration with four diffractions of the differential beams. However, the design and manufacture of a special prism brings about certain difficulties. Lu et al. (2016a) achieved a fold factor of up to 24 by diffracting the diffraction beams 12 times in an optical configuration using several prism mirrors. Because a convergent lens and mirror are complex structures and difficult to adjust, both mirrors and reflecting prism used need to adjust their incident angle. In addition, specially designed prisms are expensive, and thus a retroreflector has become the most commonly used method for double diffraction. A retroreflector can be used to make  $U$ -turns of the incident beams, leading to an easy adjustment and resistance to unexpected tips and tilts of the grating, which will be further discussed in Section 3.4.

At present, the commonly used grating pitch is approximately  $1 \mu\text{m}$ . With a four-fold optical configuration and a high electrical interpolation factor

(e.g., 4096), the resolution of a GI can be easily improved to below  $0.1 \text{ nm}$ .

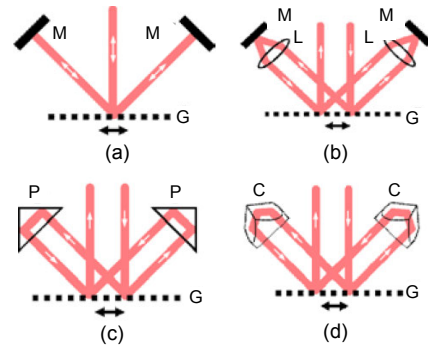


**Fig. 9 Common designs of a double-diffraction structure: (a) mirror; (b) lens and mirror; (c) prism mirror; (d) corner-cube prism**

M: mirror; G: grating; L: lens; P: prism mirror; C: corner-cube prism

### 3.2 Optical structures for large measuring ranges

In addition to an increased resolution, the measuring range is another crucial parameter that requires improvement. Although grating products can reach a length of several meters, the ruling area of a high-precision grating is still restricted to hundreds of millimeters. The range of precision of a high-density planar grating is even smaller. Apparently, such a range cannot meet the increasing measurement demand, and enlarging the measuring range is an important subject.

The most direct way to enlarge the range is to use large gratings. However, as the grating size increases, the effect of the out-of-flatness will become increasingly significant with a rapid increase in fabrication difficulty and manufacturing cost.

Thus, researchers have focused on alternatives to large-range gratings. As an effective substitution, a mosaic grating scale is used to array several small gratings together and achieve a large-scale range with a significant reduction in costs (Hosono et al., 2011; Kimura et al., 2011; Shimizu et al., 2014). To ensure the signal continuity, mosaic grating requires multiple probes to concurrently take measurements. When a gap occurs, it should be ensured that at least one probe stays in the ruling zone. Theoretically, this mosaic method can be used to realize an infinite extension. However, how to ensure the grooves of each grating to be coplanar and parallel is a major problem with

this approach. In addition to the design of a proper adjustment mechanism, a phase-difference reference window is an error compensation method (Lu et al., 2016b).

### 3.3 Optical-mechanical structure for good usability

In addition to the resolutions and measuring ranges discussed above, stability, alignment tolerance, and miniaturization of the reading head should be considered in a practical application. The improvement of these aspects will help a GI achieve good usability and obtain stable and reliable measurement results.

Grating shearing interferometer is a widely studied structure in improving stability. In general, a broad beam is obtained with a beam expander and focuses on the grating plane using a convex lens. Because the incident beam fills the region of a cone, the diffracted cone-shape beam at all levels diverges outwardly and overlaps. The spatial overlap indicates the good stability of this type of GI. Hsieh et al. (2010) proposed a polarized quasi-common-optical-path (QCOP) heterodyne GI based on the principle of a shearing interferometer.

QCOP grating interferometer is characterized by changing the polarization state using a unique semi-circular half-wave plate. Similarly, Wu et al. (2010) proposed the use of homodyne and heterodyne common-optical-path (COP) grating shearing interferometers based on a Littrow structure, which have the ability to resist environmental disturbances owing to the characteristics of the COP structure (Wu et al., 2010, 2011, 2013a, 2013c; Lee and Lu, 2011). It should be pointed out that only a small portion of the diffracted beam is taken out using a diaphragm. Therefore, a high-power laser is required to guarantee the intensity of the interference signal. Tao et al. (2015) used a collimating lens to collect a multi-order diffracted beam and constructed a reversal shearing structure, which has good beam intensity use and linearity. Based on the same principle of interference in overlapping areas of broad beams, Hsieh and Chen (2016) proposed a grating interferometer that uses a Wollaston prism to split the beams. Some mentioned grating shearing interferometer structures are shown in Fig. 10.

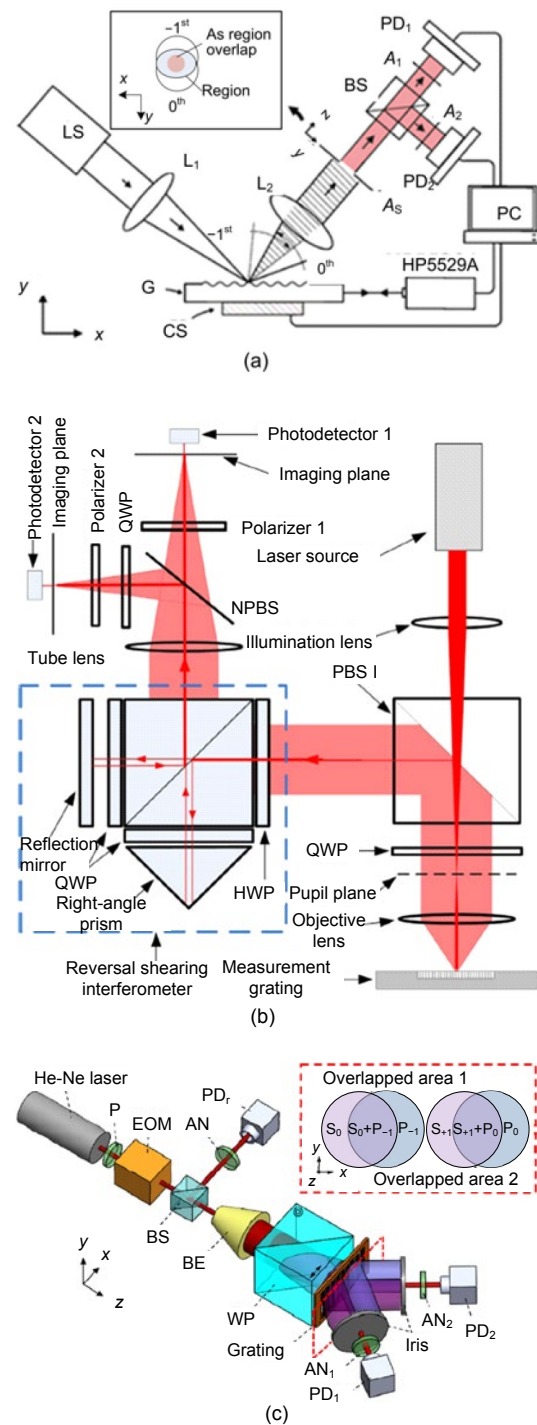


**Fig. 10** Several grating shearing interferometers: (a) a COP shearing grating interference structure (reprinted from Wu et al. (2013a), Copyright 2013, with permission from Elsevier); (b) a reversal shearing grating interference structure (reprinted from Tao et al. (2015), Copyright 2015, with permission from the Optical Society); (c) a Wollaston splitting structure (reprinted from Hsieh and Chen (2016), Copyright 2016, with permission from the Optical Society)

In the case of actual measurements, it is difficult to guarantee that grating will not shift or rotate on the unmeasured DOFs. A misalignment error and position deviation between grating and optical-reading head will lead to angular and position mismatches and finally affect the intensity of the interference signal. To reduce the systematic errors caused by the assembly, a fiber-delivered structure is used. A fiber-delivered GI uses optical fibers to connect laser source, reading head, and photodetectors, which reduces the need for a spatial light alignment with an additional advantage of moving the heat sources, such as lasers and photodetectors, away from the optical components susceptible to temperature changes (Wang et al., 2014; Xing et al., 2017; Zhu et al., 2018). In recent years, based on the fiber-delivered configuration, researchers have been exploring an all-fiber GI with a very short spatial optical path. This type of GI is slightly affected by only environmental disturbances and takes up only a small amount of space. As shown in Fig. 11, Wei et al. (2015a, 2015b) designed an all-fiber GI with a 3×3 coupler for optical interference. Šiaudinytė et al. (2018) proposed a two-DOF Littrow-type grating interferometer using monolithic fiber-fed sensor heads. Although the use of couplers to produce interference beams provides a small-space interference approach, the optical intensity transmission efficiency of optical fibers and the influence of fibers and couplers on the interference signal phase still require further study.

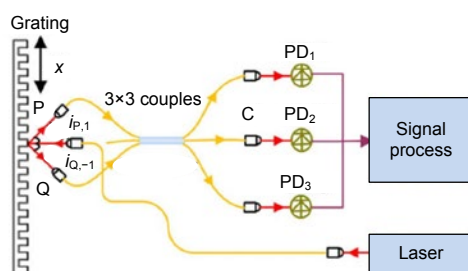


**Fig. 11** An all-fiber grating interferometer with 3×3 couplers used to attain an interference beam (reprinted from Wei et al (2015a), Copyright 2015, with permission from Chinese Laser Press)

In contrast, the use of a special optical structure can enhance the effect of interferometer in resisting an unexpected tip and tilt of the grating, for instance, in the double-diffraction structure mentioned above. Retroreflectors (Feng et al., 2013; de Groot et al.,

2016), mirrors (Wu et al., 2003, 2007), and lenses with planar mirrors (Wu et al., 1999, 2007; Lee et al., 2004; Hsu et al., 2009) are all used to improve the alignment tolerance of a GI. When grating produces an unexpected tip and tilt, the output and incident beams can be kept parallel because of the use of such a double-diffraction structure. Although a position mismatch may occur, a double-diffraction structure indeed avoids an angular mismatch, improving the alignment tolerance of a GI. As shown in Fig. 12, Chang et al. (2019) designed and quantitatively analyzed a one-DOF spatially separated heterodyne grating interferometer with a double-diffraction structure for a high alignment tolerance, and they investigated the relationship between the geometric size of the optical paths and alignment tolerance.

In addition, another common structure used to improve the alignment tolerance is a Littrow structure, which is a type of autocollimator structure (Fan et al., 2007; Kao et al., 2008; Cheng et al., 2009a; Prince, 2011; Liesener, 2013). A Littrow angle is an angle at which a non-zeroth-order diffracted beam overlaps with the incident beam of the grating. As Fig. 13 shows, a Littrow structure converts the tip and tilt of the grating into the deviation of the output beam. Kao et al. (2008) detailedly analyzed the geometric principle of a Littrow structure to improve the alignment tolerance. Wu et al. (2013d) proposed an optical structure combining a Littrow angle with a double-diffraction structure, and designed a GI with high-tolerance characteristics. In particular, a Littrow structure is not sensitive to an offset of the grating in the vertical direction. As long as the grating has a sufficient length to keep the laser spots inside the ruling area of the grating, the beam is not affected by a vertical deviation. This feature is applied to a multi-DOF GI to enlarge the measuring range in the vertical direction (Lin et al., 2015) (details will be discussed in Section 4.2).

Moreover, Akiyama and Iwaoka (1986) designed a Michelson-type Littrow structure with only a PBS and a grating. Lv et al. (2018) proposed a Littrow-type heterodyne grating interferometer for 2D measurement. This structure is convenient in terms of miniaturization.

Miniaturization is not only a method to reduce the mechanical size and to increase the usability, but also a way to reduce the effect of a misalignment by

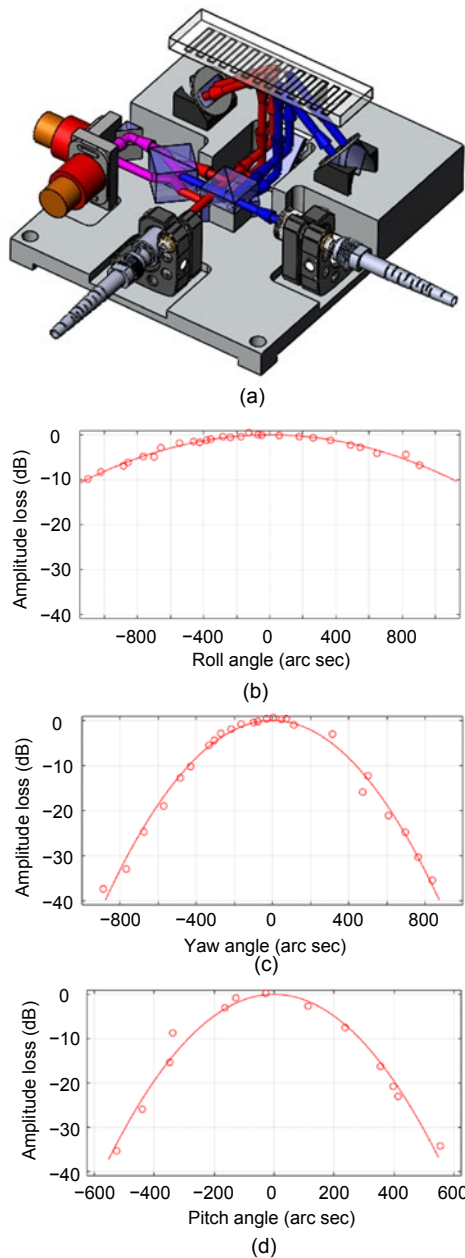


**Fig. 12** An optical configuration with mechanical fixture of a high-alignment spatially separated heterodyne grating interferometer (a), a spectrum curve roll angle and its spectrum peak curves of the measurement beam for testing the alignment tolerances in roll angle (b), a yaw angle (c), and a pitch angle (d)

shortening the length of the optical path. Currently, the size of the miniaturized GI reading heads is generally dozens of millimeters (Jourlin et al., 2002; Fan et al., 2007; Makinouchi et al., 2011; Liu and Cheng, 2012; Hsu et al., 2013). Cheng and Fan (2011) reduced the mechanical size by bonding prisms into a

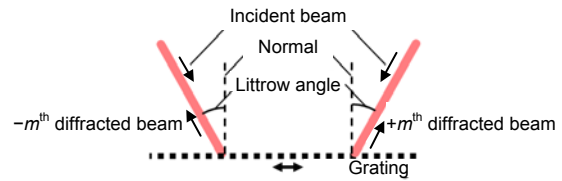


**Fig. 13** Schematic of  $\pm m^{\text{th}}$  Littrow angles and a symmetric Littrow structure

monolithic form while reducing the impact of the air gap. Liesener (2013) invented a type of compact monolithic encoder head with a hexagonal or pentagonal prism retro-reflector to replace independent corner-cube components. Shankar et al. (2007) used a natural interference region of diffracted beams to obtain the interference signal. Although the position of the PD is limited, the mirror or prism used to deflect the beams is omitted, thus reducing the complexity and size of the optical system and improving the stability to a certain extent (Shankar et al., 2007). Guo et al. (2015, 2016, 2017) and Guo and Wang (2015) proposed a self-mixing grating interferometer, whose simple optical structure has the advantage of miniaturization, where the measurement error can be controlled to within several nanometers. With the development of a micro-opto-electro-mechanical system, the use of a microstructure grating is a common approach for miniaturization of an optical-reading head. The size of the optical-reading head can be significantly reduced by integrating optoelectronic components, because the grating, PD, and optical components can be integrated into a single microstructure (Karhade et al., 2008; Shin and Kim, 2010, 2011). Zhao et al. (2011) achieved a resolution of less than 1 nm using a Michelson-type GI with a phase-sensitive diffraction grating in a microstructure.

In this section, miscellaneous methods for the improved performance of the GIs are summarized and classified into high resolution, large range, and good usability. However, it is worth emphasized that the categories are not mutually exclusive. For instance, as mentioned above, the double-diffraction configuration has the ability to double the optical fold factor and increase the alignment tolerance. By combining these enhancements with the basic structures introduced in Section 2, researchers could create different optical configurations of GIs to fulfill their project requirements.

### 4 Multi-DOF measurement approaches

With computerized numerical control, a coordinate measuring machine, a lithography machine, a Joule balance, and many other complicated apparatuses, a one-DOF linear measurement is far from sufficient. For a rigid body, the Cartesian coordinate system has six spatial DOFs (Fan et al., 2014), namely, three translational DOFs and three rotational DOFs along the  $x$ -,  $y$ -, and  $z$ -axis. To meet the actual measurement requirements, many optical structures for multi-DOF measurements have been proposed. According to the measured DOFs, these can be classified into in-plane, out-of-plane, and rotational measurements.

#### 4.1 In-plane displacement measurement

If the measurement direction of a linear GI is defined as the  $x$  axis shown in Fig. 14, the plane at where the grating is located is usually defined as the  $x$ - $y$  plane.

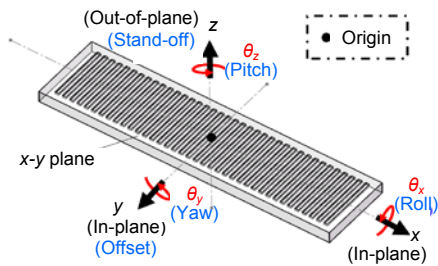


Fig. 14 Spatial six-DOF of a rigid body

The word “in-plane” indicates the  $x$ - $y$  plane. The method for upgrading a one-DOF  $x$ -displacement measurement to a two-DOF  $x$ - $y$  displacement measurement is to use two sets of perpendicular grooves to reflect the displacements in the corresponding directions. These grooves can be on different gratings (Renkens et al., 2006; Fan et al., 2011a; Kwan, 2011), in different areas of the same grating base (Wei et al., 2018), or in the same area of the same grating base, that is, the planar grating (Hsu et al., 2008). It is difficult to avoid assembly errors of different gratings, and a special fabrication is needed for ruling the grooves in different directions on the same base. Therefore, a planar grating is an optimal approach for realizing a two-DOF in-plane measurement. Fig. 15 shows several planar grating interferometers for two-DOF in-plane displacement measurement.

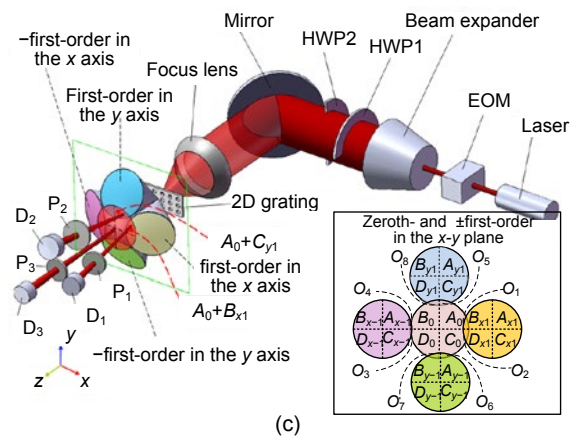
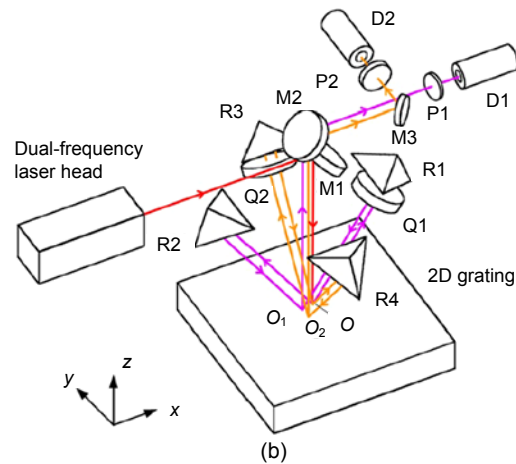
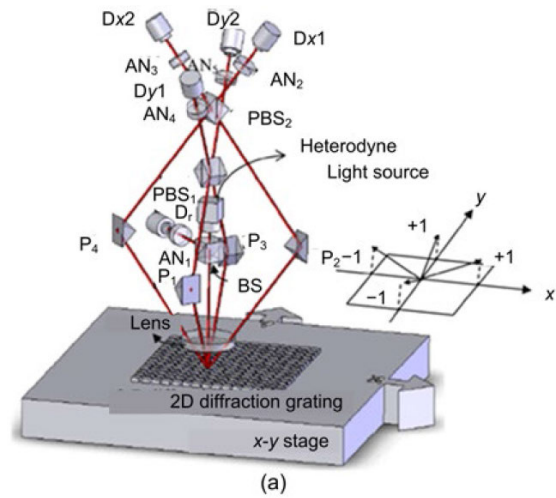


Fig. 15 Several two-DOF grating interferometer (GI) structures using planar gratings: (a) a two-DOF heterodyne GI (reprinted from Hsu et al. (2008), Copyright 2008, with permission from Elsevier); (b) a two-DOF heterodyne GI with retro-reflectors (reprinted from Feng et al. (2013), Copyright 2013, with permission from SPIE); (c) a two-DOF QCOP heterodyne grating shearing interferometer (reprinted from Hsieh et al. (2011), Copyright 2011, with permission from OSA)

According to the diffraction characteristics of a planar grating, diffracted beams will be generated in the  $x$ - and  $y$ -axis in the corresponding order. By choosing the diffracted beams in both directions and using an appropriate optical structure, displacement measurement signals in the  $x$ - and  $y$ -axis can be obtained. In fact, the various grating interferometers described in Section 2 have been developed to realize in-plane two-DOF measurements using a planar grating, such as two-DOF Littrow configurations (Hsu et al., 2008; Chung et al., 2011; Fan et al., 2011a, 2011b, 2012a), two-DOF double-diffraction configuration (Feng et al., 2013), two-DOF differential single-grating configuration (Hsu et al., 2008; Wu et al., 2008; Fan et al., 2012b; Lin et al., 2015a), and two-DOF grating shearing interferometers (Hsieh, et al., 2011; Lee JY et al., 2011; Wu et al., 2013b; Lin et al., 2015a).

However, planar gratings are limited by current manufacturing techniques, and it is difficult to rule areas of larger than one- or two-hundred millimeters at present. A large-scale grating is restricted by the out-of-flatness and pitch deviation, which results in an increase in measurement uncertainty (Gao and Kimura, 2010). Meanwhile, ruling directions of the planar grating are theoretically parallel to the  $x$ - and  $y$ -axis in the measuring plane. However, the misalignment angle in the actual assembly will mix the displacement of both directions to a certain extent, which needs to be avoided or compensated for in the signal processing module. Nonetheless, in a two-DOF GI proposed by Lin et al. (2018), the angle between the axis and grating groove was set to  $45^\circ$ , and four diffracted beams of  $(\pm 1, \pm 1)$  were used to form compound differential signals with displacements in the  $x$ - and  $y$ -axis. The left and right items of the marker represent the diffracted orders in the  $x$ - and  $y$ -axis, respectively, which means that the selected diffraction beams contain displacement information of these two directions at the same time.

## 4.2 Out-of-plane displacement measurement

In contrast to an in-plane measurement, a vertical  $z$ -axis displacement measurement is often called an “out-of-plane measurement.” Because the grating groove is orthogonal to the  $z$  axis, it cannot be directly used to measure the  $z$  displacement. This means that the reference of the  $x$ - $y$  displacement in the plane is

the grating pitch in the corresponding direction, whereas the  $z$  displacement outside the plane must use other benchmarks. For instance, a linear grating is assembled along the  $z$  axis or along the direction of the laser wavelength. For the former, a three-DOF measurement approach (Pan et al., 2013) is implemented using three linear gratings. In addition to the assembly error, mutual influence between the grating size and measurement range needs to be considered. The latter, as a combination of a laser interferometer and a grating interferometer, raises two main methods, which will be discussed later.

With the first method, all measurement beams contain phases of in-plane and out-of-plane motions. However, the phases of in-plane motions are differential, and the phases of out-of-plane motion are common. Thus, the signal processing module can decouple the displacement in different directions from these interference signals (Gao and Kimura, 2007; Kimura et al., 2010b, 2012; Ito et al., 2014; Lin et al., 2015, 2017; Lu ZG et al., 2016). As shown in Fig. 16a, with the three-DOF homodyne GI proposed by Lin et al. (2015), phase change caused by the Doppler frequency shift in the  $x$ - and  $y$ -axis is reflected in the wave equation of the  $\pm$ first-order diffracted beam as a differential form, whereas the change in the optical path caused by the  $z$  displacement has a common effect on all diffracted beams at the same time.

The other approach is to build a laser interferometer structure to measure the  $z$  displacement using a zeroth-order diffracted beam, which remains the carrier frequency (Hsieh and Pan, 2013, 2015; Lu et al., 2016; Zhang et al., 2016). Fig. 17b shows this type of two-DOF GI proposed by Lu ZG et al (2016). To measure the out-of-plane displacement, a homodyne Michelson-type interferometer with a quadratic detector module has been built.

These two methods use the principle of a laser interferometer to realize a three-DOF measurement. However, the use of a wavelength benchmark brings about a sensitivity of the  $z$ -axis measurement results to the air refractive index, and improves the environmental requirements. In addition, the optical structure for measuring the  $x$ - $y$  displacements requires as small a grating shift along the  $z$  axis as possible, which greatly limits the range of a  $z$ -axis measuring laser interferometer (generally smaller than a few

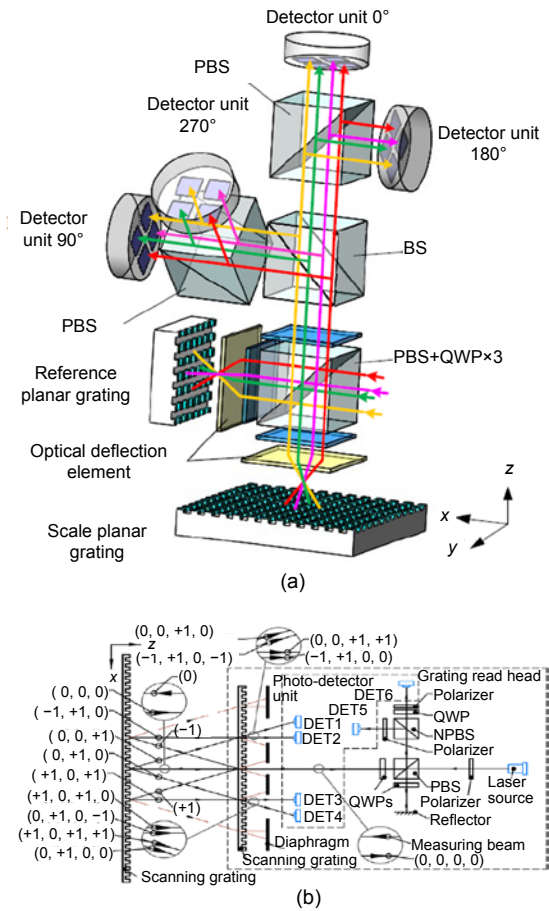


**Fig. 16** Grating interferometers using benchmarks of wavelength and grating pitch for in-plane and out-of-plane measurements: (a) a three-DOF Littrow-type GI with common  $z$ -displacement signals (reprinted from Lin et al. (2015), Copyright 2015, with permission from SPIE); (b) a two-DOF GI with an independent  $z$ -displacement interferometer (reprinted from Lu ZG et al. (2016), Copyright 2016, with permission from IOP Publishing)

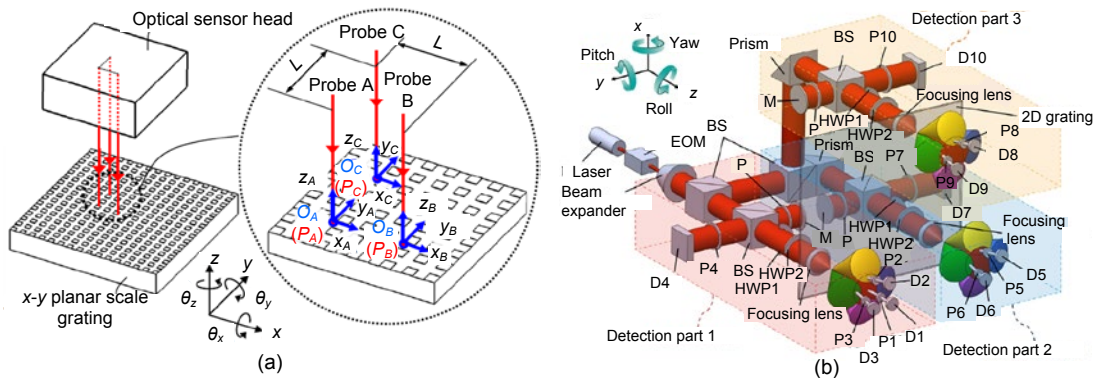


**Fig. 17** An all-grating-interferometer-based method for six-DOF measurements using three probes: (a) a six-DOF homodyne GI with three differential three-DOF probe (reprinted from Li et al. (2014), Copyright 2014, with permission from SPIE); (b) a six-DOF QCOP heterodyne GI (reprinted from Hsieh and Pan (2015), Copyright 2015, with permission from OSA)

millimeters). To solve this problem, Lin et al. (2015, 2017) combined a three-DOF homodyne GI with a Littrow structure to enlarge the  $z$  range of larger than 1 m.

### 4.3 Rotational measurement

As a diffraction optical element (DOE) capable of generating multiple beams with a specific diffracted angle, the grating is often combined with an autocollimator for angle measurements (Kim et al., 2000, 2002; Bae et al., 2001; Liu et al., 2004; Saito et al., 2009; Gao et al., 2011). Therefore, many researchers have combined the diffraction grating displacement measurement with autocollimator angle measurement into the same optical path to realize multi-DOF measurements (Huang et al., 2007; Liu et al., 2009; Lee CB et al., 2011, 2012; Liu and Cheng, 2012; Li et al., 2013). Although an autocollimator has been fully investigated, the linearity of a position sensitive device (PSD) is still a barrier to improve the angle measurement accuracy. In addition, with these methods, the measurement of angular displacement is not traceable.

For instance, in a three-DOF structure that measures translational displacement along the  $x$ - $y$  direction and the rotation angle along the  $z$  axis, two probes with a separation distance of  $L$  are used. One of them is a one-DOF probe for measuring the  $y$  displacement, whereas the other is a two-DOF probe for measuring both  $x$  and  $y$  displacements. According to the geometric relationship, the angle along the  $z$  axis can be obtained through a small-angle approximation, expressed as

$$\theta_z = \arcsin \frac{y_B - y_A}{L} \approx \frac{y_B - y_A}{L}. \quad (17)$$

Li et al. (2014) and Hsieh and Pan (2015) achieved all-interferometric six-DOF measurements using three three-DOF probes. As shown in Fig. 17, these three probes have an L-shaped layout. The translational and angular displacements of the planar grating at six DOFs can be obtained by decoupling the interference signals attained. Compared with a six-DOF laser interferometer, the optical configuration of a GI can be conveniently miniaturized (Schwenke et al., 2002).

However, how to calculate the position and posture of the grating from the raw data of these probes is important in the all-interferometric six-DOF GI. As an upgrade of the small-angle approximation, a suitable mathematical model and a complete decoupling algorithm are demanded. Wang (2017) derived and built a mathematical model based on a three-DOF  $x$ - $y$ - $\theta_z$  grating interferometer, similar to that shown in Fig. 18, for the mask stage in a lithography machine.

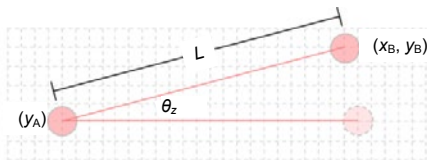


**Fig. 18 Schematic of a two-probe  $x$ - $y$ - $\theta_z$  three-DOF measurement**

The development from a one-DOF linear measurement to a six-DOF spatial positioning could be seen as an inevitable trend of GIs. In addition to the studies on the optical configurations, researchers are now focusing on the algorithms of multi-DOF GIs, especially on the error-free ones. It is not an easy task, because all the measured axes should be decoupled and almost all errors should be considered and modeled.

## 5 Error analysis

Many optical configurations of a GI for high resolution, high accuracy, and small errors have been mentioned above. Although effective, it is undeniable that such a precise and complicated grating interferometer still suffers from several errors.

### 5.1 Benchmark errors

As a benchmark, errors in the grating itself have direct effects on the measurement results. These factors have many aspects, including a ruling error, thermal expansion coefficients of the grating pitch, non-orthogonality of the planar grating, and an out-of-flatness error. Four factors are related to the material and fabrication of the grating. Under the current manufacturing conditions, there are still several ways to detect and evaluate these grating errors. In addition to the commonly used SEM and SPM, Feng et al. (2012) proposed a method to measure the orthogonality of a planar grating by combining the optical diffraction with an autocollimator principle. Gao and Kimura (2010) and Shimizu et al. (2012) proposed approaches to evaluate the out-of-flatness and pitch deviation using a Fizeau interferometer.

Hsu et al. (2013) mentioned that the pitch thermal expansion coefficients of their holographic grating are within 0.1 nm per degree of Celsius. This indicates that, to achieve an accuracy at the picometer or a higher scale, an environment with a temperature turbulence of below 0.01 °C is needed. For a calibration of the grating, a precise environment, a laser interferometer with a high accuracy, and other servicing facilities are necessary (Jakštas et al., 2005; Shu et al., 2010; Yu et al., 2015).

### 5.2 Geometric errors

For a single-DOF measurement as discussed in Sections 2 and 3, geometric errors are embodied in other five DOFs. As shown in Fig. 14, when the measured motion is along the  $x$  axis, the deviations along the  $y$  and  $z$  axes are called an offset and a stand-off error, respectively, and the rotations around the  $x$ ,  $y$ , and  $z$  axes are defined as the roll, pitch, and yaw angles, respectively. These errors can be static assembly errors and dynamic movement errors, whereas the former is a systematical error which can be calibrated and compensated for and the latter is a random error caused by actual movements of a guide rail (Xia and Fei, 2010). These errors will influence the intensity of the interference signal by creating an angular and positional mismatch of the diffracted beams.

Several optical structures for a high alignment tolerance have been discussed above. Taking a Littrow structure as an example, further analysis

reveals that, for a structure which is insensitive to only a stand-off error (Shang et al., 2016), a yaw angle in 1 arc will bring about an error within several nanometers (Fan et al., 2012b).

In fact, no optical structure can avoid the above five geometric errors at the same time. Therefore, designers have to decrease the impact of various errors in an opto-mechanical structure. For example, a coplanar design following the Abbe principle is to reduce the Abbe error (Holzapfel, 2008; Deng et al., 2018). A corresponding compensation algorithm can be adopted in the signal processing module to achieve an accurate result (Lin et al., 2013).

For a single-probe multi-DOF measuring GI, it can be seen that parts of the five error-DOFs in single-DOFs become the measured DOFs. Thus, the mutual influence among these measured DOFs should not be ignored. Taking the alignment tolerance discussed in Section 3.3 as an instance, in an optical configuration of a GI measuring translational and rotational DOFs, the significance of a high alignment tolerance is shown to keep the influence of the signal quality caused by the rotational DOFs out of the translational DOFs. For another explanation, this can be understood as maintaining the signal quality of the translational DOFs while increasing the measuring range of the rotational DOFs.

Geometric errors in the mentioned all-interferometric multi-probe grating interferometer are complicated. In addition to these errors in a single probe, a large multi-probe layout with assembly errors will bring about additional errors, which needs to be further studied.

### 5.3 Errors in signals and signal processing

For an ideal homodyne GI, the quadrature signals obtained by the photodetectors should be in perfect sinusoidal forms. In an ideal heterodyne GI, the frequency of the carrier's signal should be stable, and the quadrature signals after demodulation are perfect. However, a real photodetector's performance is far from ideal, which suffers from noises caused by parasitic parameters of the photodiode, amplifier, and printed circuit board. The temperature fluctuation influences the components and changes the features of the photodetector. Due to the existence of these noises, a high SNR is required for the resolution of interferometers, which could be attained by careful

design of the photodetectors.

In addition to noise, there are many types of signal errors, such as an unequal amplitude, DC bias, non-orthogonality of a quadrature signal, periodic nonlinear errors caused by heterodyne frequency-, polarization-, and polarization-frequency mixing (Hsieh et al., 2010; Lin et al., 2013; Olayee and Firoozjah, 2015; Olayee et al., 2017; Xing et al., 2017), non-periodic nonlinear errors caused by the grating ruling error, and linear errors caused by a wavelength drift of a dual-frequency Zeeman laser (Wang et al., 2010).

In addition to those mentioned above, many other widely used methods to reduce or eliminate these errors are applying a compensative algorithm to the signal processing module. For example, Lissajou graphs can be corrected using the Haydemann method or enhanced algorithms to obtain standard quadrature sinusoidal signals (Fan and Cheng, 2010; Hu et al., 2010, 2015; Shishova et al., 2017). In addition, an autocorrelation method was used to directly process a quadrature signal with noise (Bi and Liu, 2016), and a curve fitting method was used to smooth the results (Cheng et al., 2009b).

A main function of the signal processing module is to solve the phases from the quadrature sinusoidal signal after filtering, and then to unwrap the displacement from the phases. A method to improve the resolution during this process is an electrical interpolation (also called a "subdivision"). Common methods include a zero-crossing comparator (Ye et al., 2014), filling pulse (Wang et al., 2011, 2012), lookup table (LUT) (Dobosz, 1999), and FFT operation (Cai, 2015). As a recently prevailing method, an arctangent algorithm is an effective way to calculate the phase from sinusoidal signals acquired by analog-to-digital converters (ADC). Here, electrical interpolation factors can be as large as 40 000 (Makinouchi et al., 2011), but typically range from  $2^{12}$  to  $2^{16}$  (Holzapfel, 2008). Cai (2015) and Zhao (2016) proposed a real-time double-channel quadrature demodulation algorithm for heterodyne, and spatially separated heterodyne interferometry realized using an FPGA and 16-bit ADCs; the algorithm had already been further used to measure the nonlinearity in the area of interferometry (Fu et al., 2018a). Regardless of how large the factor is, the electrical interpolation determines the minimum phase change that can be

identified in the signal processing module, introducing a quantization error. In addition, in the signal processing module used for multi-DOF measurements, a data delay between each axis will bring about non-synchronous errors.

## 6 Conclusions and prospects

As one of the main methods for precision displacement measurement, GIs have been widely used in scientific research and industrial manufacturing. A homodyne GI with low cost, a heterodyne GI with a high SNR, and a spatially separated heterodyne GI without periodic nonlinear errors have their own specialized measurement applications.

In the development of a next-generation GI with high accuracy, a large range, and good usability, ingenious structures, such as the double-diffraction structure and a Littrow angle, have been fully studied. Structures such as an all-fiber GI and a mosaic grating have been proposed and thoroughly studied. Although new optical structures are expected to be developed, the characteristics of the grating itself will be improved with the development of fabrication techniques, such as a high density, a small uniform error, good alignment, small out-of-flatness, large groove areas, and more importantly, the improved efficiency of the diffracted light.

In terms of the multi-DOF measurements, for a measurement of less than six DOFs, the spatial six DOFs of the grating will be divided into measured and erring DOFs. How to improve the sensitivity of the former and restrain the influence of the latter are problems that must be considered by researchers and designers. For a multi-probe all-grating-interferometer based measurement method for six DOFs, although there is no erring DOF, decoupling among all DOFs still requires further mathematical modeling and experimental verification.

Finally, with the development of electrical devices and technologies, the signal processing module for a GI (and even the entire interferometer) will consider a good signal filtering performance, a wide frequency response bandwidth, a large electrical interpolation factor, and a small asynchronous error.

In any case, grating interferometers, who have rapidly grown over the past two decades, are now achieving an accuracy level at the picometer scale. In

the future, this potential measurement approach will continue to meet the ever growing scientific and industrial needs.

## References

- Akiyama K, Iwaoka H, 1986. High Resolution Digital Diffraction Grating Scale Encoder. US Patent US4629886A.
- Asano S, Goto T, Tanimura H, et al., 2001. Development of a new measurement system for straightness error by a heterodyne interferometer with a grating. Proc 10<sup>th</sup> Initiatives of Precision Engineering at the Beginning of a Millennium, p.799-803.  
[https://doi.org/10.1007/0-306-47000-4\\_157](https://doi.org/10.1007/0-306-47000-4_157)
- Badami VG, de Groot PJ, 2013. Displacement measuring interferometry. In: Harding K (Ed.), Handbook of Optical Dimensional Metrology. CRC Press, Boca Raton, USA, p.157-238.
- Badaroglu M, Ng K, Salmani M, et al., 2014. More Moore landscape for system readiness—ITRS2.0 requirements. IEEE 32<sup>nd</sup> Int Conf on Computer Design, p.147-152.  
<https://doi.org/10.1109/ICCD.2014.6974674>
- Bae EW, Kim JA, Kim SH, 2011. Multi-degree-of-freedom displacement measurement system for milli-structures. *Meas Sci Technol*, 12:1495-1502.  
<https://doi.org/10.1088/0957-0233/12/9/316>
- Bai Y, Hu PC, Lu YF, et al., 2017. A six-axis heterodyne interferometer system for Joule balance. *IEEE Trans Instrum Meas*, 66(6):1579-1585.  
<https://doi.org/10.1109/TIM.2016.2634758>
- Bi JL, Liu SB, 2016. Precision measurement of displacement with two quasi-orthogonal signals for linear diffraction grating interferometric sensors. Proc 6<sup>th</sup> Int Conf on Machinery, Materials, Environment, Biotechnology and Computer, p.25-29.  
<https://doi.org/10.2991/mmebc-16.2016.5>
- Cai HJ, 2015. Research on Picometer Resolution Phase Subdivision for Heterodyne Laser Interferometer Signals. MS Thesis, Harbin Institute of Technology, Harbin, China (in Chinese).
- Chang D, Xing X, Hu P, et al., 2019. Double-diffracted spatially separated heterodyne grating interferometer and analysis on its alignment tolerance. *Appl Sci*, 9(2): Article 263. <https://doi.org/10.3390/app9020263>
- Cheng F, Fan KC, 2011. Linear diffraction grating interferometer with high alignment tolerance and high accuracy. *Appl Opt*, 50(22):4550-4556.  
<https://doi.org/10.1364/AO.50.004550>
- Cheng F, Fan KC, Fei YT, 2009a. An improved design of the linear diffraction grating interferometer. Proc Asian Symp on Precision Engineering and Nanotechnology, p.146-149.
- Cheng F, Fei YT, Fan KC, 2009b. New method on real-time signal correction and subdivision for grating-based nanometrology. Proc 4<sup>th</sup> Int Symp on Advanced Optical Manufacturing and Testing Technologies: Design, Manufacturing, and Testing of Micro- and Nano-Optical Devices and Systems, No. 728403.  
<https://doi.org/10.1117/12.832061>

- Cho A, 2016. The long road to LIGO. *Science*, 353(6299): 534-535. <https://doi.org/10.1126/science.353.6299.534>
- Chu XC, Lü HB, Zhao SH, 2008. Research on long-range grating interferometry with nanometer resolution. *Meas Sci Technol*, 19(1):017001. <https://doi.org/10.1088/0957-0233/19/1/017001>
- Chung YC, Fan KC, Lee BC, 2011. Development of a novel planar encoder for 2D displacement measurement in nanometer resolution and accuracy. Proc 9<sup>th</sup> World Congress on Intelligent Control and Automation, p.449-453. <https://doi.org/10.1109/WCICA.2011.5970554>
- Cloud G, 2005. Optical methods in experimental mechanics, part 16: the optical Doppler effect. *Exp Tech*, 29(2):17-19. <https://doi.org/10.1111/j.1747-1567.2005.tb00207.x>
- Cosijns SJAG, Jansen MJ, 2014. Advanced optical incremental sensors: encoders and interferometers. In: Nihtianov S, Luque A (Eds.), *Smart Sensors and MEMS: Intelligent Devices and Microsystems for Industrial Applications*. Woodhead Publishing, Oxford, UK, p.230-277. <https://doi.org/10.1533/9780857099297.1.230>
- Damm C, Peschel T, Risse S, et al., 2001. Wafer stage assembly for ion projection lithography. *Microelectron Eng*, 57-58:181-185. [https://doi.org/10.1016/S0167-9317\(01\)00513-5](https://doi.org/10.1016/S0167-9317(01)00513-5)
- Deck LL, de Groot PJ, Schroeder M, 2015. Interferometric Encoder Systems. US Patent US898 869 0B2.
- de Groot PJ, Schroeder M, 2012. Interferometric Heterodyne Optical Encoder System. US Patent US2012/0194824.
- de Groot PJ, Badami VG, Liesener J, 2016. Concepts and geometries for the next generation of precision heterodyne optical encoders. Proc 31<sup>st</sup> Annual Meeting of the American Society for Precision Engineering, p.146-149.
- Deng JJ, Yan XN, Wei CL, et al., 2018. Eightfold optical encoder with high-density grating. *Appl Opt*, 57(10): 2366-2375. <https://doi.org/10.1364/AO.57.002366>
- Dobosz M, 1999. High-resolution laser linear encoder with numerical error compensation. *Opt Eng*, 38(6):968-973. <https://doi.org/10.1117/1.602137>
- Dr. Johannes Heidenhain GmbH, 2018. Exposed linear encoders. [https://www.heidenhain.com/fileadmin/pdb/media/img/208960-2E\\_Exposed\\_Linear\\_Encoders\\_en.pdf](https://www.heidenhain.com/fileadmin/pdb/media/img/208960-2E_Exposed_Linear_Encoders_en.pdf) [Accessed on Aug. 15, 2018].
- Ellis JD, 2014. *Field Guide to Displacement Measuring Interferometry*. SPIE Press, Bellingham, UK.
- Fan KC, Cheng F, 2010. LDGI signal subdivision by soft computing for nanomeasurement. Proc 6<sup>th</sup> Int Symp on Precision Engineering Measurements and Instrumentation, No. 75440I. <https://doi.org/10.1117/12.885413>
- Fan KC, Liu YS, Chen YJ, et al., 2006. A linear diffraction grating interferometer with high accuracy. Proc 3<sup>rd</sup> Int Symp on Precision Mechanical Measurements, No. 628008. <https://doi.org/10.1117/12.715260>
- Fan KC, Lai ZF, Wu P, et al., 2007. A displacement spindle in a micro/nano level. *Meas Sci Technol*, 18(6):1710-1717. <https://doi.org/10.1088/0957-0233/18/6/S07>
- Fan KC, Miao JW, Gong W, et al., 2011a. High precision measurement system based on coplanar XY-stage. Proc 7<sup>th</sup> Int Symp on Precision Engineering Measurement and Instrumentation, No. 832119. <https://doi.org/10.1117/12.904072>
- Fan KC, Lee BC, Chung YC, 2011b. A planar laser diffraction encoder in Littrow configuration for 2D nanometric positioning. *Int J Autom Smart Technol*, 1(2):93-99. <https://doi.org/10.5875/ausmt.v1i2.53>
- Fan KC, Liao BH, Chung YC, et al., 2012a. Displacement measurement of planar stage by diffraction planar encoder in nanometer resolution. Proc IEEE Int Instrumentation and Measurement Technology Conf, p.894-897. <https://doi.org/10.1109/I2MTC.2012.6229209>
- Fan KC, Zhang YL, Miao JW, et al., 2012b. Error compensation of grating interferometer due to angular error of linear stage. Proc IEEE/ASME Int Conf on advanced Intelligent Mechatronics, p.428-431. <https://doi.org/10.1109/AIM.2012.6265886>
- Fan KC, Wang HY, Yang HW, et al., 2014. Techniques of multi-degree-of-freedom measurement on the linear motion errors of precision machines. *Adv Opt Technol*, 3(4): 375-386. <https://doi.org/10.1515/aot-2014-0038>
- Feng C, Kajima M, Gonda S, et al., 2012. Accurate measurement of orthogonality of equal-period, two-dimensional gratings by an interferometric method. *Metrologia*, 49: 236-244. <https://doi.org/10.1088/0026-1394/49/3/236>
- Feng C, Zeng LJ, Wang SW, 2013. Heterodyne planar grating encoder with high alignment tolerance, especially insensitivity to grating tilts. Proc 8<sup>th</sup> Int Symp on Precision Engineering Measurement and Instrumentation, No. 87593L. <https://doi.org/10.1117/12.2012649>
- Fu HJ, Ji RD, Hu PC, et al., 2018a. Measurement method for nonlinearity in heterodyne laser interferometers based on double-channel quadrature demodulation. *Sensors*, 18(9): Article 2768. <https://doi.org/10.3390/s18092768>
- Fu HJ, Wang Y, Hu PC, et al., 2018b. Nonlinear errors resulting from ghost reflection and its coupling with optical mixing in heterodyne laser interferometers. *Sensors*, 18(3): Article 758. <https://doi.org/10.3390/s18030758>
- Gao W, 2010. *Precision Nanometrology*. Springer-Verlag London Limited, London, UK, p.69-140.
- Gao W, Kimura A, 2007. A three-axis displacement sensor with nanometric resolution. *CIRP Ann*, 56(1):529-532. <https://doi.org/10.1016/j.cirp.2007.05.126>
- Gao W, Kimura A, 2010. A fast evaluation method for pitch deviation and out-of-flatness of a planar scale grating. *CIRP Ann*, 59:505-508. <https://doi.org/10.1016/j.cirp.2010.03.035>
- Gao W, Saito Y, Muto H, et al., 2011. A three-axis autocollimator for detection of angular error motions of a precision stage. *CIRP Ann*, 60:515-518. <https://doi.org/10.1016/j.cirp.2011.03.052>
- Gao ZY, Hu JC, Zhu Y, et al., 2013. A new 6-degree-of-freedom measurement method of X-Y stages based on additional information. *Prec Eng*, 37(3):606-620. <https://doi.org/10.1016/j.precisioneng.2013.01.006>
- Gao W, Kim SW, Bosse H, et al., 2015. Measurement technologies for precision positioning. *CIRP Ann*, 64(2):773-796. <https://doi.org/10.1016/j.cirp.2015.05.009>

- Goßler S, Bertolini A, Born M, et al., 2010. The AEI 10m prototype interferometer. *Class Quant Grav*, 27(8): Article 080423.  
<https://doi.org/10.1088/0264-9381/27/8/084023>
- Guan J, Köchert P, Weichert C, et al., 2017. A differential interferometric heterodyne encoder with 30 picometer periodic nonlinearity and sub-nanometer stability. *Prec Eng*, 50:114-118.  
<https://doi.org/10.1016/j.precisioneng.2017.04.019>
- Guo DM, Wang M, 2015. Note: design of a laser feedback interferometer with double diffraction system. *Rev Sci Instrum*, 86(9):096111.  
<https://doi.org/10.1063/1.4931781>
- Guo DM, Wang M, Hao H, 2015. Displacement measurement using a laser feedback grating interferometer. *Appl Opt*, 54(31):9320-9325.  
<https://doi.org/10.1364/AO.54.009320>
- Guo DM, Wang M, Hao H, 2016. Self-mixing grating interferometer: theoretical analysis and experimental observations. *Proc Interferometry XVIII*, No. 996019.  
<https://doi.org/10.1117/12.2239519>
- Guo DM, Shi L, Yu YG, et al., 2017. Micro-displacement reconstruction using a laser self-mixing grating interferometer with multiple-diffraction. *Opt Exp*, 25(25): 31394-31406. <https://doi.org/10.1364/OE.25.031394>
- Heilmann RK, Chen CG, Konkola PT, et al., 2004. Dimensional metrology for nanometer-scale science and engineering: towards sub-nanometer accurate encoders. *Nanotechnology*, 15(10):S504-S511.  
<https://doi.org/10.1088/0957-4484/15/10/002>
- Holzapfel W, 2008. Advancements in displacement metrology based on encoder systems. *Proc 23<sup>rd</sup> Annual Meeting of the American Society for Precision Engineering*, p.1-4.
- Hori Y, Gonda S, Bitou Y, et al., 2018. Periodic error evaluation system for linear encoders using a homodyne laser interferometer with 10 picometer uncertainty. *Prec Eng*, 51:388-392.  
<https://doi.org/10.1016/j.precisioneng.2017.09.009>
- Hosono K, Kim W, Kimura A, et al., 2011. Surface encoders for a mosaic scale grating. *Int J Autom Technol*, 5(2):91-96. <https://doi.org/10.20965/ijat.2011.p0091>
- Hossein GM, Lin MJ, Horng JB, et al., 2016. Critical femto-second laser parameters for the fabrication of optimal reflecting diffraction grating on Invar36. *Opt Laser Eng*, 81:97-102.  
<https://doi.org/10.1016/j.optlaseng.2016.01.004>
- Hou WM, Zhang YB, Hu HJ, 2009. A simple technique for eliminating the nonlinearity of a heterodyne interferometer. *Meas Sci Technol*, 20(10):105303.  
<https://doi.org/10.1088/0957-0233/20/10/105303>
- Hsieh HL, Chen W, 2016. Heterodyne Wollaston laser encoder for measurement of in-plane displacement. *Opt Exp*, 24(8):8693-8707.  
<https://doi.org/10.1364/OE.24.008693>
- Hsieh HL, Pan SW, 2013. Three-degree-of-freedom displacement measurement using grating-based heterodyne interferometry. *Appl Opt*, 52(27):6840-6848.  
<https://doi.org/10.1364/AO.52.006840>
- Hsieh HL, Pan SW, 2015. Development of a grating-based interferometer for six-degree-of-freedom displacement and angle measurements. *Opt Exp*, 23(3):2451-2465.  
<https://doi.org/10.1364/OE.23.002451>
- Hsieh HL, Lee JY, Wu WT, et al., 2010. Quasi-common-optical-path heterodyne grating interferometer for displacement measurement. *Meas Sci Technol*, 21(11): 115304.  
<https://doi.org/10.1088/0957-0233/21/11/115304>
- Hsieh HL, Chen JC, Lerondel G, et al., 2011. Two-dimensional displacement measurement by quasi-common-optical-path heterodyne grating interferometer. *Opt Exp*, 19(10):9770-9782.  
<https://doi.org/10.1364/OE.19.009770>
- Hsieh HL, Lee JY, Chung YC, 2014. Wavelength-modulated heterodyne grating shearing interferometry for precise displacement measurement. *Adv Opt Technol*, 3(4):395-400. <https://doi.org/10.1515/aot-2014-0027>
- Hsu CC, Wu CC, Lee JY, et al., 2008. Reflection type heterodyne grating interferometry for in-plane displacement measurement. *Opt Commun*, 281(9):2582-2589.  
<https://doi.org/10.1016/j.optcom.2007.12.098>
- Hsu CC, Lee JY, Wu CC, 2009. Compensated laser encoder with symmetric and quasi-common-path heterodyne interferometry. *Optical Measurement Systems for Industrial Inspection*, No. 73891M.  
<https://doi.org/10.1117/12.827453>
- Hsu CC, Sung PP, Lin ZR, et al., 2013. Prototype of a compact displacement sensor with a holographic diffraction grating. *Opt Laser Technol*, 48:200-205.  
<https://doi.org/10.1016/j.optlastec.2012.10.003>
- Hsu CC, Chen H, Chiang CW, et al., 2017. Dual displacement resolution encoder by integrating single holographic grating sensor and heterodyne interferometry. *Opt Exp*, 25(24):30189-30202.  
<https://doi.org/10.1364/OE.25.030189>
- Hsu CC, Chen H, Tseng HY, et al., 2018. High displacement resolution encoder by using triple grating combination interferometer. *Opt Laser Technol*, 105:221-228.  
<https://doi.org/10.1016/j.optlastec.2018.03.005>
- Hu PC, Pollinger F, Meiners-Hagen K, et al., 2010. Fine correction of nonlinearity in homodyne interferometry. 6<sup>th</sup> Int Symp on Precision Engineering Measurements and Instrumentation, No. 75444E.  
<https://doi.org/10.1117/12.885392>
- Hu PC, Tan JB, Chen P, 2014. Double Frequency Laser Grating Interference Three-dimensional Measurement Method and System with Optical Aliasing Resistance. CN Patent CN103 604 376A (in Chinese).
- Hu PC, Zhu JH, Guo XB, et al., 2015. Compensation for the variable cyclic error in homodyne laser interferometers. *Sensors*, 15:3090-3106.  
<https://doi.org/10.3390/s150203090>
- Huang HL, Liu CH, Jywe WY, et al., 2007. Development of a three-degree-of-freedom laser linear encoder for error measurement of a high precision stage. *Rev Sci Instrum*, 78(6):066103.  
<https://doi.org/10.1063/1.2743165>

- Ito S, Aihara R, Kim WJ, et al., 2014. Three-axis vibration measurement by using a grating-interferometric vibrometer. *Adv Opt Technol*, 3(4):435-440. <https://doi.org/10.1515/aot-2014-0028>
- Jakštas A, Kaušinis S, Flügge J, 2005. Investigation of calibration facilities of precision line scales. *Mechanika*, 53(3):62-67.
- Jang YS, Kim SW, 2017. Compensation of the refractive index of air in laser interferometer for distance measurement: a review. *Int J Prec Eng Manuf*, 18(12):1881-1890. <https://doi.org/10.1007/s12541-017-0217-y>
- Jiang ML, Li FP, Wang XD, 2011. Mini-nano-displacement measurement with double diffraction grating. *Adv Mater Res*, 230-232:1159-1163. <https://doi.org/10.4028/www.scientific.net/AMR.230-232.1159>
- Jiang ML, Li FP, Wang XD, 2012. Nano-displacement measurement with grating interference. *Appl Mech Mater*, 103: 35-40. <https://doi.org/10.4028/www.scientific.net/AMM.103.35>
- Jiang ML, Li HF, Wang XD, et al., 2013. Research status and developing trends of grating nanometer measuring technology. 6<sup>th</sup> Int Symp on Precision Mechanical Measurements, No. 891631. <https://doi.org/10.1117/12.2035685>
- Jourlin Y, Jay J, Parriaux O, 2002. Compact diffractive interferometric displacement sensor in reflection. *Prec Eng*, 26:1-6. [https://doi.org/10.1016/S0141-6359\(01\)00081-2](https://doi.org/10.1016/S0141-6359(01)00081-2)
- Kao CF, Chang CC, Lu MH, 2005a. Double-diffraction planar encoder by conjugate optics. *Opt Eng*, 44(2):023603. <https://doi.org/10.1117/1.1839227>
- Kao CF, Lu SH, Lu MH, 2005b. High resolution planar encoder by retro-reflection. *Rev Sci Instrum*, 76(8):085110. <https://doi.org/10.1063/1.2006368>
- Kao CF, Lu SH, Shen HM, et al., 2008. Diffractive laser encoder with a grating in Littrow configuration. *Jpn J Appl Phys*, 47(3):1833-1837. <https://doi.org/10.1143/JJAP.47.1833>
- Karhade OG, Degertekin FL, Kurfess TR, 2008. SOI-based micro scanning grating interferometers: device characterization, control and demonstration of parallel operation. *J Micromicr*, 18(4):045007. <https://doi.org/10.1088/0960-1317/18/4/045007>
- Kilby J, 2000. The integrated circuit's early history. *Proc IEEE*, 88(1):109-111. <https://doi.org/10.1109/5.811607>
- Kim JA, Kim KC, Bae EW, et al., 2000. Six-degree-of-freedom displacement measurement system using a diffraction grating. *Rev Sci Instrum*, 71(8):3214-3219. <https://doi.org/10.1063/1.1305816>
- Kim JA, Bae EW, Kim SH, et al., 2002. Design methods for six-degree-of-freedom displacement measurement systems using cooperative targets. *Prec Eng*, 26(1):99-104. [https://doi.org/10.1016/S0141-6359\(01\)00105-2](https://doi.org/10.1016/S0141-6359(01)00105-2)
- Kim P, Kim D, You K, 2012. Adaptive compensation for the nonlinearity error in a heterodyne interferometer. *J Korean Phys Soc*, 61(11):1759-1765. <https://doi.org/10.3938/jkps.61.1759>
- Kimura A, Gao W, Arai Y, et al., 2010a. Design and construction of a two-degree-of-freedom linear encoder for nanometric measurement of stage position and straightness. *Prec Eng*, 34(1):145-155. <https://doi.org/10.1016/j.precisioneng.2009.05.008>
- Kimura A, Gao W, Zeng LJ, 2010b. Position and out-of-straightness measurement of a precision linear air-bearing stage by using a two-degree-of-freedom linear encoder. *Meas Sci Technol*, 21:054005. <https://doi.org/10.1088/0957-0233/21/5/054005>
- Kimura A, Hosono K, Kim WJ, et al., 2011. A two-degree-of-freedom linear encoder with a mosaic scale grating. *Int J Nanomanuf*, 7(1):73-91. <https://doi.org/10.1504/IJNM.2011.039964>
- Kimura A, Gao W, Kim WJ, et al., 2012. A sub-nanometric three-axis surface encoder with short-period planar gratings for stage motion measurement. *Prec Eng*, 36(4): 576-585. <https://doi.org/10.1016/j.precisioneng.2012.04.005>
- Kunzmann H, Pfeifer T, Flügge J, 1993. Scales vs. laser interferometers performance and comparison of two measuring systems. *CIRP Ann*, 42(2):753-767. [https://doi.org/10.1016/S0007-8506\(07\)62538-4](https://doi.org/10.1016/S0007-8506(07)62538-4)
- Kwan YBP, 2011. Lithographic Apparatus, Device Manufacturing Method and Device Manufactured Thereby. US Patent US794 039 2.
- Lan HB, Ding YC, Liu HZ, et al., 2007. Review of the wafer stage for nanoimprint lithography. *Microelectron Eng*, 84(4):684-688. <https://doi.org/10.1016/16/j.mee.200.2007.01.002>
- Lazar J, Čip O, Čížek M, et al., 2010. Multiaxis interferometric system for positioning in nanometrology. Proc 9<sup>th</sup> WSEAS Int Conf on Microelectronics, Nanoelectronics, Optoelectronics, p.92-95.
- Lee CB, Lee SK, 2013. Multi-degree-of-freedom motion error measurement in an ultraprecision machine using laser encoder. *Rev J Mech Sci Technol*, 27(1):141-152. <https://doi.org/10.1007/s12206-012-1217-6>
- Lee CB, Kim GH, Lee SK, 2011. Design and construction of a single unit multi-function optical encoder for a six-degree-of-freedom motion error measurement in an ultraprecision linear stage. *Meas Sci Technol*, 22(10): 105901. <https://doi.org/10.1088/0957-0233/22/10/105901>
- Lee CB, Kim GH, Lee SK, 2012. Uncertainty investigation of grating interferometry in six degree-of-freedom motion error measurements. *Int J Prec Eng Manuf*, 13(9):1509-1515. <https://doi.org/10.1007/s12541-012-0199-8>
- Lee CK, Wu CC, Chen SJ, et al., 2004. Design and construction of linear laser encoders that possess high tolerance of mechanical runout. *Appl Opt*, 43(31):5754-5762. <https://doi.org/10.1364/AO.43.005754>
- Lee JY, Lu MP, 2011. Optical heterodyne grating shearing interferometry for long-range positioning applications. *Opt Commun*, 284(1):857-862. <https://doi.org/10.1016/j.optcom.2010.09.079>
- Lee JY, Jiang GA, 2013. Displacement measurement using a wavelength phase-shifting grating interferometer. *Opt Exp*, 21(21):25553-25564. <https://doi.org/10.1364/OE.21.025553>
- Lee JY, Chen HY, Hsu CC, et al., 2007. Optical heterodyne grating interferometry for displacement measurement

- with subnanometric resolution. *Sens Actuat A*, 137(1): 185-191. <https://doi.org/10.1016/j.sna.2007.02.017>
- Lee JY, Hsieh HL, Lerondel C, et al., 2011. Heterodyne grating interferometer based on a quasi-common-optical path configuration for a two-degrees-of-freedom straightness measurement. *Appl Opt*, 50(9):1272-1279. <https://doi.org/10.1364/AO.50.001272>
- Lee TH, 2007. The (pre-) history of the integrated circuit: a random walk. *IEEE SSCS News*, 12(2):16-22. <https://doi.org/10.1109/N-SSC.2007.4785573>
- Li XH, Gao W, Muto H, et al., 2013. A six-degree-of-freedom surface encoder for precision positioning of a planar motion stage. *Prec Eng*, 37(3):771-781. <https://doi.org/10.1016/j.precisioneng.2013.03.005>
- Li XH, Shimizu Y, Ito T, et al., 2014. Measurement of six-degree-of-freedom planar motions by using a multiprobe surface encoder. *Opt Eng*, 53(12):122405. <https://doi.org/DOI:10.1117/1.OE.53.12.122405>
- Li Q, Liu X, Zhao L, et al., 2017. A novel vibration sensor based on phase grating interferometry. *Appl Phys B*, 123(5): Article 162. <https://doi.org/10.1007/s00340-017-6724-9>
- Liesener J, 2013. Compact Encoder for Interferometric Encoder System. US Patent US201 311 406 2A1.
- Lin CB, Yan SH, Wei C, et al., 2013. Optimized design and error analysis of optical system for heterodyne grating interferometry. Int Conf on Optical Instruments and Technology: Optoelectronic Measurement Technology and Systems, No. 90460C. <https://doi.org/10.1117/12.2037576>
- Lin CB, Yan SH, Du ZG, et al., 2015a. High-efficiency gold-coated cross-grating for heterodyne grating interferometer with improved signal contrast and optical subdivision. *Opt Commun*, 339:86-93. <https://doi.org/10.1016/j.optcom.2014.11.059>
- Lin CB, Yan SH, Du ZG, et al., 2015b. Symmetrical short-period and high signal-to-noise ratio heterodyne grating interferometer. *Chin Opt Lett*, 13(10):100501. <https://doi.org/10.3788/COL201513.100501>
- Lin CB, Yan SH, Ding D, et al., 2018. Two-dimensional diagonal-based heterodyne grating interferometer with enhanced signal-to-noise ratio and optical subdivision. *Opt Eng*, 57(6):064102. <https://doi.org/10.1117/1.OE.57.6.064102>
- Lin DJ, Jiang H, Yin C, 2000. Analysis of nonlinearity in a high-resolution grating interferometer. *Opt Laser Technol*, 32(2):95-99. [https://doi.org/10.1016/S0030-3992\(00\)00022-0](https://doi.org/10.1016/S0030-3992(00)00022-0)
- Lin J, Guan J, Wen F, et al., 2015. Grating encoder for wide range three-axis displacement measurement. 9<sup>th</sup> Int Symp on Precision Engineering Measurement and Instrumentation, No. 944602. <https://doi.org/10.1117/12.2082475>
- Lin J, Guan J, Wen F, et al., 2017. High-resolution and wide range displacement measurement based on planar grating. *Opt Commun*, 404:132-138. <https://doi.org/10.1016/j.optcom.2017.03.012>
- Liu CH, Cheng CH, 2012. Development of a grating based multi-degree-of-freedom laser linear encoder using diffracted light. *Sens Actuat A*, 181:87-93. <https://doi.org/10.1016/j.sna.2012.05.004>
- Liu CH, Jywe WY, Tzeng SC, 2004. Simple three-dimensional laser angle sensor for three-dimensional small-angle measurement. *Appl Opt*, 43(14):2840-2845. <https://doi.org/10.1364/AO.43.002840>
- Liu CH, Huang HL, Lee HW, 2009. Five-degrees-of-freedom diffractive laser encoder. *Appl Opt*, 48(14):2767-2777. <https://doi.org/10.1364/AO.48.002767>
- Lu YC, Zhou CH, Li S, et al., 2016a. Study of a grating interferometer with high optical subdivision technique. Holography, Diffractive Optics, and Applications VII, No. 1002214. <https://doi.org/10.1117/12.2246091>
- Lu YC, Wei CL, Jia W, et al., 2016b. Two-degree-of-freedom displacement measurement based on a short period grating in symmetric Littrow configuration. *Opt Commun*, 380:382-386. <https://doi.org/10.1016/j.optcom.2016.06.016>
- Lu YX, Qi XD, Li XT, et al., 2016. Removal of all mosaic grating errors in a single-interferometer system by a phase-difference reference window. *Appl Opt*, 55(28): 7997-8002. <https://doi.org/10.1364/AO.55.007997>
- Lu ZG, Wei PP, Wang CQ, et al., 2016. Two-degree-of-freedom displacement measurement system based on double diffraction gratings. *Meas Sci Technol*, 27(7): 074012. <https://doi.org/10.1088/0957-0233/27/7/074012>
- Lv Q, Liu ZW, Wang W, et al., 2018. Simple and compact grating-based heterodyne interferometer with the Littrow configuration for high-accuracy and long-range measurement of two-dimensional displacement. *Appl Opt*, 57(31):9455-9463. <https://doi.org/10.1364/AO.57.009455>
- Makinouchi S, Watanabe A, Takasaki M, et al., 2011. An evaluation of a modulated laser encoder. *Prec Eng*, 35(2): 302-308. <https://doi.org/10.1016/j.precisioneng.2010.11.008>
- Olayee S, Firoozjah AG, 2015. Modeling the nonlinearity of polarizing beam splitters in nano-displacement measurement of laser encoder using Jones matrix analysis. Proc 13<sup>th</sup> Int Conf on Telecommunications, p.1-6. <https://doi.org/10.1109/ConTEL.2015.7231188>
- Olayee S, Firoozjah AG, Naraghi A, 2017. Mathematically modeling of imperfect polarized laser beam in laser encoders for automotive applications. Proc 5<sup>th</sup> Int Conf on Control, Instrumentation, and Automation, p.44-48. <https://doi.org/10.1109/ICCIAutom.2017.8258651>
- Pan SW, Hsieh HL, Wang WC, 2013. 6-DOF displacement and angle measurements using heterodyne laser encoder. Instrumentation, Metrology, and Standards for Nanomanufacturing, Optics, and Semiconductors VII, No. 881909. <https://doi.org/10.1117/12.2024082>
- Post D, 1971. Moiré fringe multiplication with a nonsymmetrical doubly blazed reference grating. *Appl Opt*, 10(4): 901-907. <https://doi.org/10.1364/AO.10.000901>
- Prince J, 2011. Compact Littrow Encoder. US Patent US786 433 6.
- Ramm P, Klumpp A, Weber J, et al., 2010. 3D system-on-chip technologies for more than Moore systems. *Microsyst Technol*, 16(7):1051-1055. <https://doi.org/10.1007/s00542-009-0976-1>

- Renkens MJM, Struycken AM, Kok RJ, et al., 2006. Lithographic Apparatus, Measurement System, and Device Manufacturing Method. US Patent US710 272 9.
- Richardson C, Tsuriya M, Fu H, 2017. Technology roadmap overviews and future direction through technology gaps. Int Conf on Electronics Packaging, p.35-40. <https://doi.org/10.1109/ICEP-IAAC.2015.7111028>
- Riemer O, 2011. Advances in ultra precision manufacturing. Proc Int Symp on Ultraprecision Engineering and Nanotechnology, p.1-6
- Ronchi V, 1964. Forty years of history of a grating interferometer. *Appl Opt*, 3(4):437-451. <https://doi.org/10.1364/AO.3.000437>
- Saito Y, Arai Y, Gao W, 2009. Detection of three-axis angles by an optical sensor. *Sensors Actuat A*, 150(2):175-183. <https://doi.org/10.1016/j.sna.2008.12.019>
- Schmidt RHM, 2012. Ultra-precision engineering in lithographic exposure equipment for the semiconductor industry. *Phil Trans R Soc A*, 370(1973):3950-3972. <https://doi.org/10.1098/rsta.2011.0054>
- Schwenke H, Neuschaefer-Rube U, Pfeifer T, et al., 2002. Optical methods for dimensional metrology in production engineering. *CIRP Ann*, 51(2):685-699. [https://doi.org/10.1016/S0007-8506\(07\)61707-7](https://doi.org/10.1016/S0007-8506(07)61707-7)
- Shang P, Xia HJ, Fei YT, 2016. High-resolution diffraction grating interferometric transducer of linear displacements. 7<sup>th</sup> Int Symp on Precision Mechanical Measurements, No. 99031I. <https://doi.org/10.1117/12.2212280>
- Shankar A, Tanwar LS, Sirohi RS, 2007. High resolution and low run-out errors in displacement measuring grating interferometer using natural interference zone. *J Opt*, 36(3):111-122. <https://doi.org/10.1007/BF03354822>
- Shibazaki Y, Kohno H, Hamatani M, 2009. An innovative platform for high-throughput, high-accuracy lithography using a single wafer stage. Proc SPIE, Optical Micro-lithography XXII, No. 72741I. <https://doi.org/10.1117/12.813386>
- Shimizu Y, Kim WJ, Ito S, et al., 2012. Form error characterization of reflective-type gratings. *Key Eng Mater*, 523-524:859-864. <https://doi.org/10.4028/www.scientific.net/KEM.523-524.859>
- Shimizu Y, Ito T, Li X, et al., 2014. Design and testing of a four-probe optical sensor head for three-axis surface encoder with a mosaic scale grating. *Meas Sci Technol*, 25(9):094002. <https://doi.org/10.1088/0957-0233/25/9/094002>
- Shin D, Kim B, 2010. An optical encoder using micromachined two gratings with phase. Proc ASME Int Mechanical Engineering Congress & Exposition, p.479-483. <https://doi.org/10.1115/IMECE2010-40392>
- Shin D, Kim B, 2011. A laser interferometer encoder with two micromachined gratings generating phase-shifted quadrature. *J Micromech Microeng*, 21(8):085036. <https://doi.org/10.1088/0960-1317/21/8/085036>
- Shishova MV, Odinokov SB, Lushnikov DS, et al., 2017. Mathematical modeling of signal transfer process into optical system of a linear displacement encoder. *Proc Eng*, 201:623-629. <https://doi.org/10.1016/j.proeng.2017.09.676>
- Shu XM, Zuo Y, Xu XB, 2010. Error correction technology of the length grating measuring system. Proc 6<sup>th</sup> Int Symp on Precision Engineering Measurements and Instrumentation, No. 75442G. <https://doi.org/10.1117/12.885868>
- Šiaudinytė L, Molnar G, Köning R, et al., 2018. Multi-dimensional grating interferometer based on fibre-fed measurement heads arranged in Littrow configuration. *Meas Sci Technol*, 29(5):054007. <https://doi.org/10.1088/1361-6501/aaa8b4>
- Tan JB, Hu PC, Xing X, 2014. Double Frequency Laser Grating Interference Two-dimensional Measurement Method. CN Patent CN103 604 375A (in Chinese).
- Tao Z, Tan JB, Cui JW, 2015. Linear response, multi-order grating interferometry using a reversal shearing imaging system. *Opt Lett*, 40(19):4552-4555. <https://doi.org/10.1364/OL.40.004552>
- Teimel A, 1991. Technology and application of grating interferometers in high-precision measurement. Progress in Precision Engineering. Springer-Verlag, Berlin, Germany, p.15-30. [https://doi.org/10.1016/0141-6359\(92\)90003-F](https://doi.org/10.1016/0141-6359(92)90003-F)
- Wang GC, Xie XD, Yan SH, 2010. Influence of non-ideal performance of lasers on displacement precision in single grating heterodyne interferometry. Proc 5<sup>th</sup> Int Symp on Advanced Optical Manufacturing and Testing Technologies, No. 76562X. <https://doi.org/10.1117/12.864195>
- Wang GC, Yan SH, Yang DX, et al., 2011. An interference signal processing method for displacement measurement by dual wavelength and single grating. 7<sup>th</sup> Int Symp on Precision Engineering Measurement and Instrumentation, No. 83211A. <https://doi.org/10.1117/12.904076>
- Wang GC, Yan SH, Zhou WH, et al., 2012. Dynamic tracking down-conversion signal processing method based on reference signal for grating heterodyne interferometer. *Opt Eng*, 51(8):081512. <https://doi.org/10.1117/1.OE.51.8.081512>
- Wang J, 2017. Research on 3-DOF Grating Interference Measurement Model of Mask Table. MS Thesis, Harbin Institute of Technology, Harbin, China (in Chinese).
- Wang LJ, Zhang M, Zhu Y, et al., 2014. A novel heterodyne grating interferometer system for in-plane and out-of-plane displacement measurement with nanometer resolution. Proc 29<sup>th</sup> Annual Meeting of the American Society for Precision Engineering, p.173-177.
- Wang XZ, Dong XH, Guo J, et al., 2004. Two-dimensional displacement sensing using a cross diffraction grating scheme. *J Opt A Pure Appl Opt*, 6(1):106-111. <https://doi.org/10.1088/1464-4258/6/1/019>
- Wei CH, Yan SH, Lin CB, et al., 2015a. Compact grating displacement measurement system with a 3×3 coupler. *Chin Opt Lett*, 13(5):051301. <https://doi.org/10.3788/COL201513.051301>
- Wei CH, Yan SH, Lin CB, et al., 2015b. Signal processing for single grating displacement measurement based on 3×3 coupler. Proc 9<sup>th</sup> Int Symp on Precision Engineering Measurement and Instrumentation, No. 944625. <https://doi.org/10.1117/12.2180922>
- Wei PP, Lu X, Qiao DC, et al., 2018. Two-dimensional displacement measurement based on two parallel gratings. *Rev Sci Instrum*, 89(6):065105.

- <https://doi.org/10.1063/1.5024637>
- Williams RP, Hord SK, Hall NA, 2017. Optically read displacement detection using phase-modulated diffraction gratings with reduced zeroth-order reflections. *Appl Phys Lett*, 110(15):151104. <https://doi.org/10.1063/1.4979541>
- Wise S, Quetschke V, Deshpande AJ, et al., 2005. Phase effects in the diffraction of light: beyond the grating equation. *Phys Rev Lett*, 95(1):013901. <https://doi.org/10.1103/PhysRevLett.95.013901>
- Wu CC, Chen YC, Lee CK, et al., 1999. Design verifications of a linear laser encoder with high head-to-scale tolerance. Current Developments in Optical Design and Optical Engineering VIII, p.73-82. <https://doi.org/10.1117/12.368194>
- Wu CC, Chang CC, Kao CF, et al., 2003. Novel planar laser encoder system for two-dimensional positioning with ultra high head-to-scale alignment tolerance. Current Developments in Lens Design and Optical Engineering IV, p.55-63. <https://doi.org/10.1117/12.504442>
- Wu CC, Wu WJ, Pan ZS, et al., 2007. Laser linear encoder with both high fabrication and head-to-scale tolerances. *Appl Opt*, 46(16):3169-3176. <https://doi.org/10.1364/AO.46.003169>
- Wu CC, Hsu CC, Lee JY, et al., 2008. Optical heterodyne laser encoder for in-plane nanopositioning. Interferometry XIV: Techniques and Analysis, No. 70631A. <https://doi.org/10.1117/12.793710>
- Wu CC, Cheng CY, Yang ZY, 2010. Optical homodyne common-path grating interferometer with subnanometer displacement resolution. Interferometry XV: Applications, No. 779105. <https://doi.org/10.1117/12.860513>
- Wu CC, Hsu CC, Lee JY, et al., 2011. Common-path laser encoder for nanopositioning in long travel range. Proc SICE Annual Conf, p.817-820.
- Wu CC, Yang JS, Cheng CY, et al., 2013a. Common-path laser encoder. *Sens Actuat A*, 189:86-92. <https://doi.org/10.1016/j.sna.2012.08.034>
- Wu CC, Chen YZ, Liao CH, 2013b. Common-path laser planar encoder. *Opt Exp*, 21(16):18872-18883. <https://doi.org/10.1364/OE.21.018872>
- Wu CC, Hsu CC, Lee JY, et al., 2013c. Heterodyne common-path grating interferometer with Littrow configuration. *Opt Exp*, 21(11):13322-13332. <https://doi.org/10.1364/OE.21.013322>
- Wu CC, Hsu CC, Lee JY, et al., 2013d. Littrow-type self-aligned laser encoder with high tolerance using double diffractions. *Opt Commun*, 297:89-97. <https://doi.org/10.1016/j.optcom.2013.01.048>
- Xia HJ, Fei YT, 2010. Precise stage design with planar diffraction grating interferometer. Proc 6<sup>th</sup> Int Symp on Precision Engineering Measurements and Instrumentation, No. 754411. <https://doi.org/10.1117/12.885215>
- Xie JD, Yan LP, Chen BY, et al., 2017. Iterative compensation of nonlinear error of heterodyne interferometer. *Opt Exp*, 25(4):4470-4482. <https://doi.org/10.1364/OE.25.004470>
- Xing X, Chang D, Hu PC, et al., 2017. Spatially separated heterodyne grating interferometer for eliminating periodic nonlinear errors. *Opt Exp*, 25(25):31384-31393. <https://doi.org/10.1364/OE.25.031384>
- Yan SH, Wang GC, Lin CB, et al., 2015. Displacement measurement by single-grating heterodyne interferometry. Proc 11<sup>th</sup> Conf on Lasers and Electro-Optics Pacific Rim, p.1-2.
- Ye GY, Fan SJ, Liu HZ, et al., 2014. Design of a precise and robust linearized converter for optical encoders using a radiometric technique. *Meas Sci Technol*, 25(12):125003. <https://doi.org/10.1088/0957-0233/25/12/125003>
- Yu HY, Liu HZ, Li X, et al., 2015. Calibration of non-contact incremental linear encoders using a macro-micro dual-drive high-precision comparator. *Meas Sci Technol*, 26(9): Article 095103. <https://doi.org/10.1088/0957-0233/26/9/095103>
- Yuan JL, Lyu BH, Hang W, et al., 2017. Review on the progress of ultra-precision machining technologies. *Front Mech Eng*, 12(2):158-180. <https://doi.org/10.1007/s11465-017-0455-9>
- Zhang M, Zhu Y, Wang LJ, et al., 2016. Two-DOF Heterodyne Grating Interferometer Displacement Measurement System. US Patent US013 890 3A1.
- Zhang M, Zhu Y, Ni C, et al., 2017. Two-DOF Heterodyne Grating Interferometer Displacement Measurement System. CN Patent CN106 289 068A (in Chinese).
- Zhao B, Wang L, Xu ME, et al., 2015. A displacement measuring system based on grating double diffraction. Proc 9<sup>th</sup> Int Symp on Precision Engineering Measurement and Instrumentation, No. 94464J. <https://doi.org/10.1117/12.2182024>
- Zhao JL, 2016. Key Technology of Signal Processing in Heterodyne Laser Interferometry with Pico Meter Resolution. MS Thesis, Harbin Institute of Technology, Harbin, China (in Chinese).
- Zhao SS, Hou CL, Bai J, et al., 2011. Nanometer-scale displacement sensor based on phase-sensitive diffraction grating. *Appl Opt*, 50(10):1413-1416. <https://doi.org/10.1364/AO.50.001413>
- Zherdev AY, Odinkov SB, Lushnikov DS, et al., 2017. Optical position encoder on four-section diffraction grating. Proc SPIE, Holography: Advances and Modern Trends, No. 102331I. <https://doi.org/10.1117/12.2264801>
- Zhu Y, Zhang M, Wang LJ, et al., 2014. Dual-Frequency Grating Interferometer Displacement Measurement System. WO Patent WO201 407 180 6A1.
- Zhu Y, Zhang M, Wang LJ, et al., 2018. Dual-frequency Grating Interferometer Displacement Measurement System. US Patent US988 556 B2.